Dissolution kinetics of diopside as a function of solution saturation state: Macroscopic measurements and implications for modeling of geological storage of CO_2

Damien Daval [a,b,*], Roland Hellmann [c], Jérôme Corvisier [b], Delphine Tisserand [c], Isabelle Martinez [a], François Guyot [a,d]

[a] *Institut de Physique du Globe de Paris, Centre de Recherches sur le Stockage Géologique du CO2, 4 Place Jussieu, 75005 Paris, France*
[b] *Laboratoire de Géologie, UMR 8538 du CNRS, École Normale Supérieure, 24 Rue Lhomond, 75005 Paris, France*
[c] *Géochimie de l'Environnement, Laboratoire de Géophysique Interne et Tectonophysique, CNRS UMR C5559, OSUG, Université Joseph Fourier, 38041, Grenoble Cedex 9, France*
[d] *Institut de Minéralogie et de Physique des Milieux Condensés, CNRS, Université Paris 6 et 7, 140 rue de Lourmel 75252, Paris, France*

Abstract

Measurements of the dissolution rate of diopside (r) were carried out as a function of the Gibbs free energy of the dissolution reaction (ΔG_r) in a continuously stirred flow-through reactor at 90 °C and $pH_{90\ °C} = 5.05$. The overall relation between r and ΔG_r was determined over a free energy range of $-130.9 < \Delta G_r < -47.0$ kJ mol^{-1}. The data define a highly non-linear, sigmoidal relation between r and ΔG_r. At far-from-equilibrium conditions ($\Delta G_r \leqslant -76.2$ kJ mol^{-1}), a rate plateau is observed. In this free energy range, the rates of dissolution are constant, independent of [Ca], [Mg] and [Si] concentrations, and independent of ΔG_r. A sharp decrease of the dissolution rate ($\sim$1 order of magnitude) occurs in the transition ΔG_r region defined by $-76.2 < \Delta G_r \leqslant -61.5$ kJ mol^{-1}. Dissolution closer to equilibrium ($\Delta G_r > -61.5$ kJ mol^{-1}) is characterised by a much weaker inverse dependence of the rates on ΔG_r. Modeling the experimental r–ΔG_r data with a simple classical transition state theory (TST) law as implemented in most available geochemical codes is found inappropriate. An evaluation of the consequences of the use of geochemical codes where the r–ΔG_r relation is based on basic TST was carried out and applied to carbonation reactions of diopside, which, among other reactions with Ca- and Mg-bearing minerals, are considered as a promising process for the solid state sequestration of CO_2 over long time spans. In order to take into account the actual experimental r–ΔG_r relation in the geochemical code that we used, a new module has been developed. It reveals a dramatic overestimation of the carbonation rate when using a TST-based geochemical code. This points out that simulations of water–rock–CO_2 interactions performed with classical geochemical codes should be evaluated with great caution.
© 2010 Elsevier Ltd. All rights reserved.

1. INTRODUCTION

A long-standing objective in the study of the kinetics of water–rock interactions has consisted in attempting to link mineral dissolution and precipitation rates determined in laboratory experiments to the corresponding rates measured in the field. Bridging the gap between the laboratory and field scales has remained a challenge for several decades now. As an example, discrepancies of up to four orders of magnitude have been determined for dissolution, where the kinetics are considerably faster in laboratory reactors compared to rates measured in the field (e.g. Brantley, 1992; Swoboda-Colberg and Drever, 1993; Drever and Clow, 1995; White and Brantley, 2003). However, since

---

* Corresponding author. Address: Institut de Physique du Globe de Paris, Centre de Recherches sur le Stockage Géologique du CO2, 4 Place Jussieu, 75005 Paris, France.
  E-mail address: daval@ipgp.jussieu.fr (D. Daval).

the laboratory approach is the only one which allows for the rigorous determination of the dependence of mineral weathering rates on the primary rate-controlling parameters (e.g. pH, temperature, or reactive surface area), laboratory-based rate laws are practically always input in geochemical codes to model long-term mineral and fluid evolution during water–rock interactions (e.g. Xu et al., 2004; Knauss et al., 2005; Goddéris et al., 2006; Daval et al., 2009a). As a consequence, one must be aware that such modeling efforts can potentially be the source of substantial overestimations of "true" mineral weathering rates. The consequences of such overestimations may be dramatic, especially when dealing with pressing environmental topics, such as the fate of anthropogenic gases (e.g. CO_2) stored in geological reservoirs, or the evolution of far-field geological systems surrounding confined nuclear wastes.

Overcoming these presumed rate-overestimations requires assessing their possible sources. A detailed review of this topic is beyond the scope of this study; nevertheless, the main ideas that have been debated are briefly discussed here. It has been proposed that reactions in the field are slower than predicted because of (1) the effect of "aging" of the mineral surfaces, resulting either from the rapid disappearance of the most reactive high-energy lattice defects or from the passivating effect of protective secondary phases (Eggleston et al., 1989; Velbel, 1993; Nugent et al., 1998; White and Brantley, 2003), (2) the omitted presence of solutes having a strong inhibiting effect (e.g. Al species, Oelkers et al., 1994) or (3) the fact that many water–rock (mineral) interactions occur at saturation indices approaching chemical equilibrium (Stefánsson and Arnórsson, 2000), deriving their driving force from relatively small free energy differences (e.g. Pačes, 1972; White and Brantley, 2003). According to some authors, this effect may be inadequately taken into account in geochemical codes (e.g. Lasaga and Lüttge, 2001). This latter point will be discussed further on.

A general form of the rate law which links the kinetics of mineral dissolution/precipitation to the major rate-controlling parameters of the reaction can be written as follows (Lasaga, 1995; see also Aagaard and Helgeson, 1982):

$$r' = k_0 \exp(-E_a/RT)A_{min}g(I)\Pi a_i^{ni}f(\Delta G_r) \qquad (1)$$

In this equation, r' (mol s^{-1}) is the overall dissolution/precipitation rate, k_0 (mol s^{-2} s^{-1}) is the rate constant that incorporates pre-exponential factors in the Arrhenius relation, E_a (J mol^{-1}) is the activation energy, R (J mol^{-1} K^{-1}) and T (K) are the ideal gas constant and temperature, respectively, A_{min} (m^2) is the reactive surface area. In accordance with Eq. (1), which implies a linear dependence of the dissolution rate on A_{min}, most studies dealing with dissolution kinetics of minerals report the values of normalised dissolution rates (r, expressed in mol m^{-2} s^{-1}). The $g(I)$ term stands for a possible dependence of the rate on the ionic strength (I) of the solution. The Πa_i^{ni} term expresses the effect of aqueous species that promote (in particular H$^+$ or OH$^-$) or inhibit the overall reaction. The $f(\Delta G_r)$ term is a function which accounts for the effect on the rate of how far from chemical equilibrium (ΔG_r) the reaction takes place. Among the different rate-controlling parameters of Eq. (1), the $f(\Delta G_r)$ term has surely been the least studied

up to now. This follows from the experimental complexity of conducting and acquiring data at close-to-equilibrium conditions. In lieu of experimentally-based rate-free energy relations, most geochemical models use a theoretical relation established within the framework of transition state theory (TST) (e.g. Xu et al., 2004; Knauss et al., 2005) that is (e.g. Eyring, 1935a,b; Lasaga, 1981):

$$f(\Delta G_r) = 1 - \exp(\Delta G_r/RT) \qquad (2)$$

As one can note, such a mathematical relation entails that the mineral dissolution (or precipitation) rate is roughly independent of ΔG_r over a wide free energy range far-from-equilibrium (i.e. $f(\Delta G_r) \approx 1$), whereas it decreases sharply over a very narrow range of ΔG_r values close-to-equilibrium (e.g. at 90 °C, $f(\Delta G_r) > 0.95$ as long as $\Delta G_r < -10$ kJ mol^{-1}). As far as we know, such a dependence of the dissolution rate on the Gibbs free energy of reaction has strictly been observed for two silicates only: kaolinite (e.g. Nagy et al., 1991) and quartz (e.g. Berger et al., 1994). On another hand, there is growing evidence from new available experimental data that r–ΔG_r relations for silicate dissolution can significantly diverge from this simplest TST-based $f(\Delta G_r)$ relation. Several studies (Burch et al., 1993; Devidal et al., 1997; Cama et al., 2000; Taylor et al., 2000; Hellmann and Tisserand, 2006; Beig and Lüttge, 2006; Hellmann et al., 2007, in press; Dixit and Carroll, 2007) have reported highly non-linear relations that are characterised by a sharp decrease of the dissolution rate (up to one order of magnitude) even at very negative ΔG_r values, such as ~ -40 kJ/mol for albite (Burch et al., 1993; Hellmann and Tisserand, 2006) and labradorite (Taylor et al., 2000). The conceptual model for such divergences from the simple TST-based relation remains a source of debate. On one hand, some authors have tried to accommodate the differences between experimental observations and the simple TST-based relation by elaborating TST-like functions (e.g. Gautier et al., 1994; Oelkers et al., 1994; Devidal et al., 1997); on the other hand, others (e.g. Burch et al., 1993; Lasaga and Lüttge, 2001) have proposed a complete re-interpretation of the observed r–ΔG_r features. Whatever the correct model is, it appears that the basic TST r–ΔG_r relations actually implemented in most geochemical codes lead to incorrect estimates of actual reaction rates (see e.g. discussion in Daval et al., 2009a). Determining experimentally empirical rate–free energy relationships for the dissolution of minerals is thus of crucial importance for avoiding potential overestimations of mineral weathering rates determined by numerical modeling of water/rock interactions.

Geological storage of CO_2, one of the possible strategies for mitigating against rising levels of anthropogenic CO_2 in the atmosphere, is among those fields of study which will heavily rely on modeling, as the fate of CO_2 after injection will have to be estimated over long time spans (typically $>10^5$ years, e.g. Lackner, 2003). Mineral carbonation reactions of basic and ultrabasic rocks, which can be considered as one of the safest options for the geological sequestration of CO_2 (e.g. Oelkers et al., 2008), involves processes where the dependence of the weathering rates of silicates upon ΔG_r is fundamental. The overall aqueous carbonation of

(ultra)basic minerals, which can be written as follows (where M is a divalent species):

$$M_xSi_yO_{x+2y-z}(OH)_{2z} + xCO_2$$
$$\rightarrow xMCO_3 + ySiO_2 + zH_2O \quad (3)$$
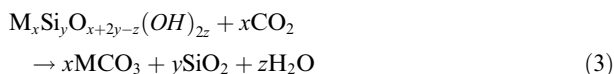
can be divided into two principal steps, namely silicate dissolution and production of metal and bicarbonate ion:

$$M_xSi_yO_{x+2y-z}(OH)_{2z} + 2xCO_2$$
$$\rightarrow xM^{2+} + 2xHCO_3^- + ySiO_2 + (z-x)H_2O \quad (4)$$
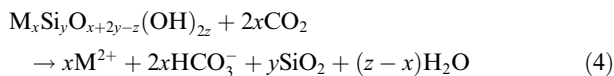
(note that in the above equation, CO_2 forms carbonic acid, which in turn produces protons) and carbonate precipitation:

$$xM^{2+} + 2xHCO_3^- \rightarrow xMCO_3 + xH2O + xCO_2 \quad (5)$$
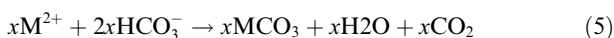
The role of precipitation of secondary phases on the overall carbonation rate has been a debated question: on the one hand, amorphous silica and/or carbonates can act as passivating coatings which inhibit or slow down dissolution of the primary silicates (e.g. Shih et al., 1999; Béarat et al., 2006; Stockmann et al., 2008; Daval et al., 2009a,b); on the other hand, the rapid precipitation of secondary phases (as is the case for calcite precipitation compared to dissolution of Ca-bearing silicates) controls the composition of the aqueous phase and fixes the free energy of the dissolution reaction at very negative values, thus potentially promoting its rate (e.g. Daval et al., 2009a with respect to carbonation reaction; Murakami et al., 1998; Putnis, 2002 with respect to other dissolution or replacement reactions). The accurate knowledge of the effective $f(\Delta G_r)$ function used in the framework of Eq. (1) is obviously essential for the adequate modeling of such reactions in series.

These questions are the primary motivation for this study of the r–ΔG_r relationship for diopside, one of the most common minerals constituting basic and ultrabasic rocks. Diopside is a pyroxene with a nominal composition of $CaMgSi_2O_6$. While almost all of the aforementioned studies dedicated to the rate–free energy relationships were conducted on feldspars or clays, only a few were devoted to other minerals (e.g. Dixit and Carroll, 2007; Davis et al., 2008). Moreover, diopside was chosen because its dissolution behaviour and the dependence of its dissolution rate on surface area, temperature, pH, and organic ligands have been studied over almost 30 years (Schott et al., 1981; Knauss et al., 1993; Chen and Brantley, 1998; Golubev and Pokrovsky, 2006). In addition, its importance in carbonation processes has been highlighted in several recent studies (e.g. McGrail et al., 2006; Stockmann et al., 2008). Finally, the first part of our work, which is reported in the present study, can be considered to be complementary to the study of Dixit and Carroll (2007), which was also based on the effect of saturation state on diopside dissolution. As was the case with their experiments, the dissolution experiments were conducted either in initially (Ca, Mg, Si)-free solutions, or in (Ca, Mg, Si)-enriched input solutions.

The originality of the present study is based on the following specificities: (1) our investigations were carried out over a more extended range of Gibbs free energies, thereby allowing for the first time to unequivocally test for the existence of an extended dissolution rate plateau, similarly to the study of Hellmann and Tisserand (2006) in the case of albite feldspar; (2) dissolution of diopside was investigated over very long durations (up to ~2500 h), this criterion being fundamental (especially for diopside, as quoted in Chen and Brantley, 1998) to ensure that true steady-state rates are reached; (3) we used pH buffer solutions for which the specific effect upon diopside dissolution rate is particularly well documented (Golubev and Pokrovsky, 2006); (4) the chosen pH was slightly acidic in order to more closely approach conditions of CO_2 sequestration, which allowed us to measure dissolution rates at much higher degrees of undersaturation (i.e. more negative values of ΔG_r); (5) the experimental temperature was 90 °C (compared to 125–175 °C in Dixit and Carroll's study, 2007), which is closer to the usually accepted upper bound for CO_2 sequestration (Bachu, 2002); (6) comparing a simple TST-based free energy function (Eq. (2)) with the experimental one determined in the present study allowed us to quantitatively assess the rates of carbonation of Ca-bearing silicates, based on geochemical simulations. The present study will be complemented by an upcoming study that will present investigations on the evolution of the fluid-mineral (diopside) interface as a function of ΔG_r from the μm to nm-scale which will provide a better understanding of the mechanisms of diopside dissolution as a function of ΔG_r.

2. MATERIALS AND METHODS

2.1. Starting materials

The diopside used in this study came from Mererani (Tanzania) and was purchased from Mawingu Gems. It consists of cm-sized translucent, pale green crystals of gem quality, with only a very small, non-quantifiable amount of a black phase identified to be graphite by Raman spectroscopy. Because of its different colour, graphite was easily removed by hand picking. No other minor phases were evidenced with the analytical techniques we used (i.e. Raman spectroscopy, X-ray diffraction and scanning electron microscopy). The chemical composition of the diopside was determined by electron microprobe and is listed in Table 1. Samples were initially crushed and sieved to recover the 300–500 μm-sized fraction. The powder was then ultrasonically cleaned in absolute ethanol for 10 min in order to remove fine particles; the cloudy supernatant was removed and replaced with fresh alcohol. This process was repeated five times until the supernatant became clear. The diopside was then rinsed with ultrapure deionised water (18.2 MΩ cm^{-1}) for 5 min and dried overnight in air at 40 °C. The efficacy of this procedure was monitored by scanning electron microscopy (SEM), which revealed only a few fine particles still adhering on the surface. The specific surface area (SSA) of the powder was determined to be 0.028 m^2 g^{-1} based on a three-point BET method using Kr as the absorbent gas; the estimated accuracy being 30%. The use of powders with such a coarse grain size facilitated the circulation of fluid between the grains and thereby minimised chemical gradients with the bulk reactor fluid.

Table 1
Chemical composition of diopside from electron microprobe analysis (in wt.%).

SiO_2	Al_2O_3	CaO	Cr_2O_3	MnO	FeO	Na_2O	MgO	Total
55.27	0.71	26.43	0.07	0.42	0.12	0.17	18.11	101.29

In most experiments, the surface coverage of the bottom of the reactor vessel by diopside crystals was sparse enough to ensure single layers of grains. In addition, coarse grains facilitate post-experimental surface studies using electron microscopy and spectroscopy techniques.

2.2. Experimental apparatus

The experiments were conducted in a continuously stirred hydrothermal flow-through system (CSTR), using a 50 ml Parr reactor (for a detailed description, see Hellmann et al., 1997). To minimise corrosion, the system incorporates Ti components (reactor, impellor, and tubing). A Knauer HPLC Smartline 1000 pump, with a minimum flow rate capability of 0.001 ml min^{-1}, was used to inject fluid into the reactor. All experiments were conducted at 90 °C and at 2–2.5 MPa fluid pressure. At these P–T conditions, only a single liquid phase is present in the reactor. The solution in the reactor was always well mixed due to the rotating impellor, but its speed was adjusted to avoid the entrainment of the grains into a suspended slurry.

2.3. Reactor input solutions

The dissolution reactions were carried out at 90 °C and at $pH_{(90 °C)} = 5.05 \pm 0.10$. As already mentioned, working with a slightly acidic pH allowed us to investigate diopside dissolution kinetics over an extended range of ΔG_r, and also to mitigate against the precipitation of secondary phases, in particular Mg-bearing phyllosilicates, zeolites, and carbonate minerals. It is well known that the substantial presence of precipitates ultimately complicates interpretation of r–ΔG_r relations. All chemical reagents used were of high quality (analytical grade or better), including the ultrapure deionised water (18.2 MΩ cm^{-1}). The input solutions were based on an acetate pH buffer, using 0.0064 mol l^{-1} sodium acetate and 0.005 mol l^{-1} acetic acid. The pH was measured with a Mettler pH electrode calibrated initially with commercial buffer solutions (pH 4.00, 7.00 at 20 °C) and adjusted (if needed) to 4.75 ($\pm$0.05) at 20 °C using small additions of either dilute HCl or dilute NaOH solutions. The use of an acetate buffer is a key point of our experimental set-up. As has been generally considered, and experimentally shown recently for diopside (Golubev and Pokrovsky, 2006), anionic ligands can promote the dissolution rate of silicates. As a consequence, the use of buffers in general, and in particular of organic buffers, is not recommended for accurately determining the dependence of silicate dissolution rates upon specific parameters, other than the organic ligand itself (see e.g. discussion in Brantley and Chen, 1995). Nonetheless, they have been widely used in many of the previously cited studies on dissolution rate-free energy relations. In the present study, the buffer concentration was chosen such that the effect of the acetate

ligand was negligible, according to Golubev and Pokrovsky (2006) (the acetate concentration was calculated to never exceed 0.008 mol l^{-1} at the end of each run). The main drawback of working with relatively dilute buffers is that the buffering capacity of the solution is weak. To reach conditions closer to equilibrium, as well as to initiate experiments at specific free energy values, solutions containing variable amounts of $CaCl_2$, $MgCl_2$, and sodium metasilicate ($Na_2SiO_3 \cdot 9H_2O$, which spontaneously dissolves in water to produce SiO_2(aq), Na^+ and OH^- species) were also prepared, such that the composition of the input solutions is stoichiometric. The pH of this solution was adjusted to ~4.75 by addition of dilute HCl solution, before introducing 0.064 mol l^{-1} sodium acetate and 0.005 mol l^{-1} acetic acid. If needed, the pH was adjusted again to 4.75 ($\pm$0.05) at 20 °C using small additions of either dilute HCl or dilute NaOH solutions. The pH of the input and output solutions was measured periodically. The in situ pH of the solution was calculated using the thermodynamic module of the CHESS code (van der Lee and de Windt, 2002), based on the EQ3/6 database. Running the CHESS code with the following solution composition: [acetic acid] = 0.0114 mol l^{-1}, [Na^+] = 0.0064 mol l^{-1} and achieving the electrical balance on [H^+], yielded an input solution pH of 4.75 at 20 °C, or 4.94 at 90 °C. The in situ $pH_{(90 °C)}$ of each solution was recalculated using either (1) the measured concentrations of dissolved species as supplementary inputs and achieving the electrical balance on [H^+] or (2) the measured output pH at 20 °C extrapolated to 90 °C with the CHESS code. As reported in Table 2, these two methods gave pH values which were in excellent agreement, never exceeding differences of 0.09 pH units. On the whole, the experiments were all conducted at $pH_{(90 °C)} = 5.05 \pm 0.10$. The calculated ionic strength of the output solutions was between 0.01 and 0.02 mol l^{-1} (90 °C).

2.4. Experimental protocol and analytical procedures

The experimental procedures applied in the present study are similar to those used by Hellmann and Tisserand (2006). The results reported here represent a series of experiments that were run over a total period of ~3 years. The dissolution rates were measured over a very extended range of Gibbs free energies of >80 kJ mo1^{-1} (from −130.9 to −47.0 kJ mol^{-1}). As detailed above, diopside was crushed in several different batches and washed, the grain size of each batch being kept constant from one experiment to another to avoid the introduction of an additional source of uncertainties in the determination of dissolution rates. The ΔG_r for each experiment was controlled in three ways: (1) by the mass of solid in the reactor (increasing the mass corresponds to reactions at higher ΔG_r values); (2) by the fluid residence time, which was controlled by the flow rate (the lower the flow rate, the higher the residence time, and thus the closer to equilibrium the dissolu-

Table 2
Summary of experimental and calculated data concerning the dissolution of diopside.

Expt.	Time	m_0	v	$[Ca]_{in}$	$[Mg]_{in}$	$[Si]_{in}$	$[Ca]_{out}$	$[Mg]_{out}$	$[Si]_{out}$	$pH^{in}_{(20\,°C)}$	$pH^{out}_{(20\,°C)}$	$pH^a_{in\ situ}$	$pH^b_{in\ situ}$	r_{Ca}	r_{Mg}	r_{Si}	r_{Avg}	ΔG_r^a	ΔG_r^b
DPS-A1	25	0.6579	9.2E-06	0	0	0	1.85	4.03	4.33	4.78	4.83	4.93	4.97	9.10E-10	2.09E-09	1.09E-09	1.00E-09[c]	−131.4	−130.3
DPS-A2	29	0.6579	1.6E-06	0	0	0	9.10	11.0	19.3	4.78	4.82	4.94	4.97	7.91E-10	1.00E-09	8.59E-10	8.84E-10	−114.5	−113.5
DPS-B	23	0.6632	8.0E-07	0	0	0	17.9	19.3	42.0	4.80	4.79	4.96	4.94	7.61E-10	8.64E-10	9.18E-10	8.48E-10	−105.4	−106.2
DPS-C	38	0.6379	1.6E-07	0	0	0	85.7	85.6	201	4.77	4.80	4.96	4.95	7.52E-10	7.91E-10	9.03E-10	8.16E-10	−86.8	−87.2
DPS-D	36	0.7056	8.0E-08	0	0	0	214	214	463	4.74	4.78	5.00	4.94	8.64E-10	9.08E-10	9.58E-10	9.10E-10	−75.3	−77.0
DPS-E	75	0.7056	3.2E-08	0	0	0	312	308	633	4.74	4.78	5.04	4.93	5.08E-10	5.27E-10	5.28E-10	5.21E-10	−69.8	−73.0
DPS-F	69	1.41180	3.2E-08	0	0	0	345	336	694	4.76	4.90	5.09	5.05	2.77E-10	2.84E-10	2.85E-10	2.82E-10	−67.5	−68.8
DPS-G	97	1.41180	1.6E-08	0	0	0	471	464	1027	4.76	5.01	5.16	5.15	1.87E-10	1.94E-10	2.10E-10	1.97E-10	−61.2	−61.7
DPS-H	44	0.9789	8.2E-08	268	274	520	455	453	867	4.70	4.80	4.95	4.95	5.53E-10	5.57E-10	5.25E-10	5.45E-10	−68.7	−68.7
DPS-I	47	0.9789	3.3E-08	268	274	520	640	633	1191	4.70	4.85	5.04	4.99	4.40E-10	4.46E-10	4.07E-10	4.31E-10	−62.2	−63.5
DPS-J	122	1.6218	1.5E-08	268	274	520	917	919	1629	4.70	4.99	5.16	5.11	2.19E-10	2.29E-10	1.92E-10	2.14E-10	−55	−56.4
DPS-K	41	1.0260	3.1E-08	1809	1704	3597	1926	1824	3597	4.70	4.92	4.95	5.05	1.24E-10	1.32E-10	−2.62E-14	1.28E-10[d]	−51.7	−48.9
DPS-L	92	1.0238	1.5E-08	1869	1777	3468	1856	2028	3178	4.80	4.95	4.99	5.08	−6.32E-12	1.33E-10	−7.47E-11	1.33E-10[e]	−47.9[f]	−46.1[g]

In the first four columns are reported the name of the experiment, its total duration time (days), the initial mass of diopside (grams) and the flow rate of the pump ($l\,s^{-1}$). The input ($[Ca]_{in}$, $[Mg]_{in}$ and $[Si]_{in}$) and output ($[Ca]_{out}$, $[Mg]_{out}$ and $[Si]_{out}$) solution compositions are indicated in the six following columns (μM). The pH of the input and output solutions measured at room temperature are reported in the columns labelled $pH^{in}_{(20\,°C)}$ and $pH^{out}_{(20\,°C)}$. These values were used to calculate the *in situ* pH basing either (a) on the initial pH and the effluent concentration of species or ($pH^a_{in\ situ}$) (b) on the outlet pH measured at 20 °C ($pH^b_{in\ situ}$). The dissolution rates based on each major constituting element of diopside, as well as the unweighted average of the dissolution rate are reported in the subsequent columns ($mol\,m^2\,s^{-1}$). In the two last columns are mentioned the ΔG_r values ($kJ\,mol^{-1}$) at which the steady-state dissolution rates were measured, based either on $pH^a_{in\ situ}$ or on $pH^b_{in\ situ}$. (c) Rate based on Si and Ca release only, the value of $[Mg]_{out}$ being doubtful (possible contamination of the external tubing, which was changed after experiment); (d) based on Ca and Mg only; (e) based on Ca only; (f) and (g) calculated values supposing a congruent dissolution process (see text for details).

tion reaction); (3) by adding stoichiometric amounts of dissolved Ca, Mg and Si species to the input solution. The time period of each experimental run ranged from at least ~600 h (25 days) at far-from-equilibrium conditions to ~2500 h (15 weeks) at conditions closest to equilibrium. The chosen length of a particular run served to ensure the attainment of an hydrodynamic steady-state (based on the injection of a minimum of 2–3 reactor volumes), and more importantly, a chemical steady-state, as determined by relatively constant rates of release of Ca, Mg and Si with time (i.e. when the trend of the outlet concentrations as a function of time were scattered, rather than monotonic, and when the dispersion of the data was undistinguishable from the estimated analytical uncertainties). Such long durations are especially needed for diopside dissolution, as already observed by Chen and Brantley (1998). In some experiments, after the attainment of steady-state concentrations, the flow rate was changed to (a) new value(s) during the course of the experiment (referred to as multiple flow rate experiments). The exit solution from each experiment was collected periodically in order to determine the rates of dissolution as a function of time, and especially to ascertain whether constant concentrations (i.e., steady-state rates) were achieved. The inlet and outlet concentrations of dissolved species were measured by ICP-AES (Perkin–Elmer Optima 3300 DV) using matrix-matched standards and matrix blanks. Measurements of the output pH were compared to the theoretical values, and this was then used to estimate the uncertainties on the *in situ* pH. The analytical uncertainties in the ICP-AES measurements, based on repeated analyses of standard solutions and blanks, were estimated to be better than ±10% (typically 6–7%). Both the pH and dissolved species concentration uncertainties were used to estimate ΔG_r uncertainties.

2.5. Experimental calculation of dissolution rates

Diopside dissolution rates for each experiment can be retrieved using the variations of [Ca], [Mg] and [Si] between inlet and outlet solutions of the reactor. The following mass balance for any aqueous species can be applied to CSTR systems (adapted from e.g. Hänchen et al., 2006):

$$V \times \frac{d\Delta[i]}{dt} = -v \times \Delta[i] + \eta_i \times r_i' \qquad (6)$$

In the above equation, V is the volume of the reactor (expressed in l), $\Delta[i]$ is the difference between the effluent and influent concentrations of a solute i (mol l^{-1}), v is the flow rate (l s^{-1}), η_i is the stoichiometric coefficient of element i in the mineral, r_i' is the dissolution rate of diopside (mol s^{-1}) determined with respect to the ith species of diopside. Because the rates of dissolution determined at the end of each run (or before a flow rate change during multiple flow rate experiments) represent steady-state rates (i.e., $d\Delta[i]/dt = 0$), Eq. (6) can be re-written in simplified form as follows:

$$r_i = \frac{v \times \Delta[i]}{\eta_i \times SSA \times m_0} \qquad (7)$$

where m_0 is the initial mass of diopside (g), such that r_i is expressed in mol m^2 s^{-1}. Note that rigorously, the dissolution rate should be normalised by the diopside surface area

at any time t during the experiment, i.e. $SSA_t \times m_t$. In some studies the dissolution rates are normalised with respect to post-dissolution specific surface areas (e.g. see discussion in Chen and Brantley, 1998). However, this was not done here because the measurement of post-dissolution specific surface areas can be altered by interference from porous altered surface layers (e.g., Casey et al., 1989) that are not representative of the surface area of the dissolving mineral surface. The calculated error in the *absolute* values of dissolution rates is largely attributable to the terms SSA and $\Delta[i]$ (note, however, that the SSA term does not influence the *relative* comparison between one rate and another as the grain size of the diopside batches was kept constant from one experiment to another). The relative decrease of the mass loss of a given diopside batch never exceeded 4%, such that its effect on the reactive surface area was considered to be insignificant. Representative errors in r_{Ca}, r_{Mg}, and r_{Si} were calculated and are discussed further on.

2.6. Theoretical calculations

Aqueous speciation, ion activity, pH, and the Gibbs free energy of the reaction at 90 °C were calculated with CHESS (van der Lee and de Windt, 2002) using the EQ3/6 database. At acidic pH conditions, dissolution of diopside can be written as follows:

$$CaMgSi_2O_6 + 4H^+ \rightarrow Ca^{2+} + Mg^{2+} + 2H_2O + 2SiO_2(aq) \qquad (8)$$
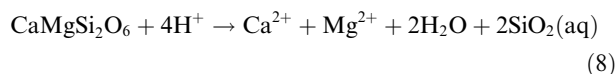
The Gibbs free energy for the above dissolution reaction is calculated from:

$$\Delta G_r = RT \times \ln\left(\frac{a_{Ca^{2+}} \times a_{Mg^{2+}} \times a_{SiO_2(aq)}^2}{K_{eq} \times a_{H^+}^4}\right) \qquad (9)$$

where K_{eq} is the equilibrium constant and a_i stands for the activity of the ith species. Activity coefficients for aqueous species were calculated using the Davies equation. Evaluation of the dissolution reaction given by Eq. (8) is based on pure diopside with unit activity. No attempt was made to experimentally determine the equilibrium constant of the diopside dissolution in this study. The equilibrium constant was calculated by the code using an extrapolation of integrated equilibrium constants between 0 and 300 °C.

As one can note, ΔG_r is strongly dependent upon H$^+$. Because the experiments were carried out at ~pH 5, this had the advantage that rates could be investigated over a greater range of far-from-equilibrium conditions (i.e. more highly negative free energies) compared to the study by Dixit and Carroll (2007). Conversely, in the present study we were not able to approach equilibrium conditions as closely as in this previous study.

3. RESULTS AND DISCUSSION

3.1. Behaviour of elemental release from non-steady to steady-state as a function of ΔG_r

The typical evolution of cation (Ca, Mg, or Si) concentrations as a function of time are shown in Fig. 1, with ΔG_r representative of the three different r–ΔG_r regions evidenced
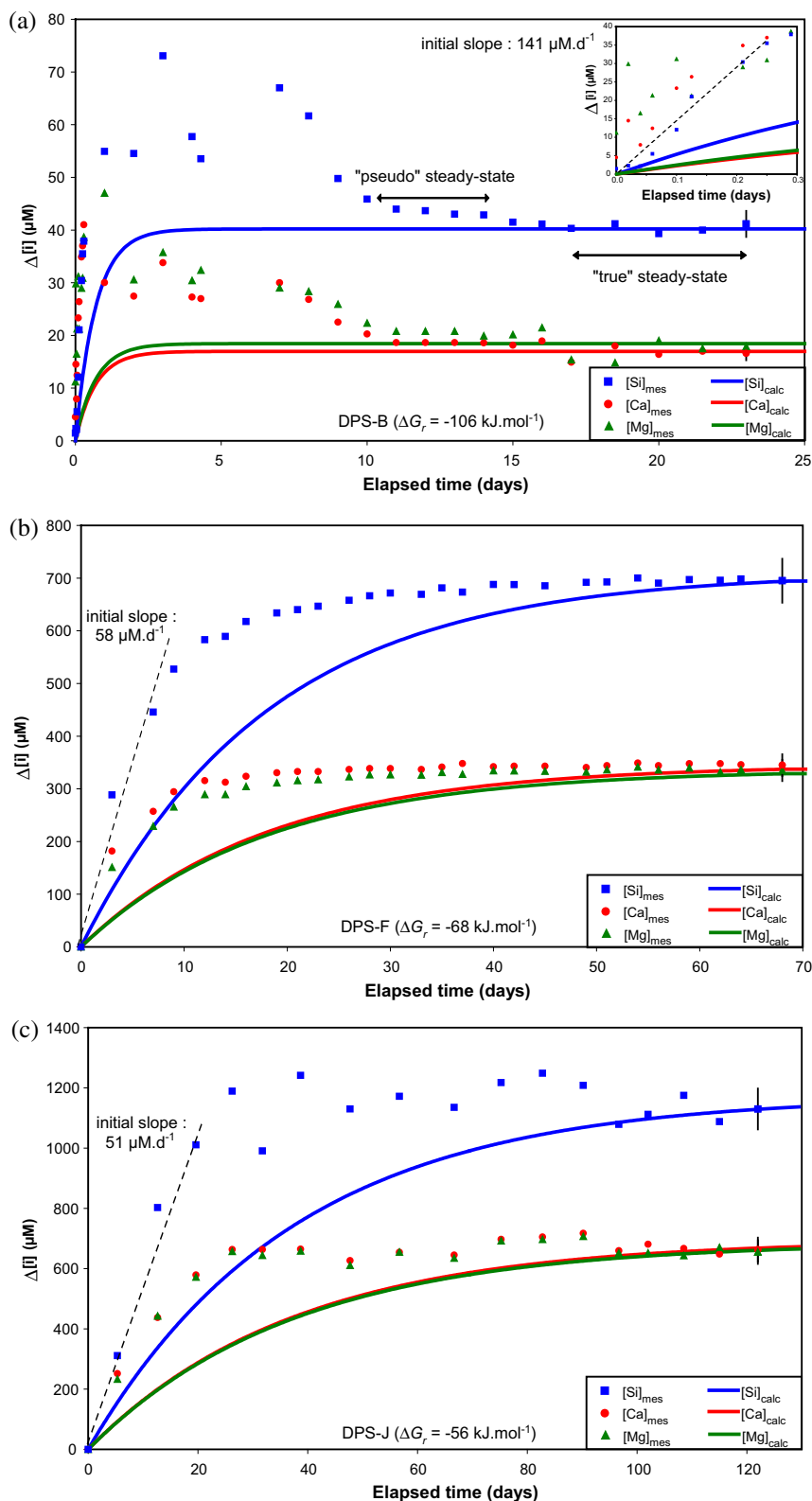
Fig. 1. Time evolution of Ca, Mg and Si concentrations (see legend) as a function of ΔG_r defined at steady-state conditions for experiments (a) DPS-B, (b) DPS-F and (c) DPS-J. The solid lines represent the time evolution expected based on a constant dissolution rate of diopside (see text for details).

in the present study (see details in Section 3.3). To better assess the time dependence of cation release (and thus, the

time dependence of the diopside dissolution rate), the data are compared with modelled curves representing the theo-

retical cation release if the diopside dissolution rate was constant over the course of each experiment. These curves were calculated by integrating Eq. (6) with the initial condition $\Delta[i](t = 0) = 0$ and obtaining r'_i from the concentrations plateaus at the end of experiments (v and η_i are known), leading to the following solution:

$$\Delta[i](t) = \left(\frac{-r'_i \times \eta_i}{v}\right) \exp\left(\frac{-v}{V}t\right) + \left(\frac{r'_i \times \eta_i}{v}\right) \qquad (10)$$

A common feature of these three graphs, irregardless of the value of ΔG_r, is that the experimental data points lie systematically above the modelled curves for all three cations (Ca, Mg, Si). This indicates that the apparent dissolution rate of diopside is initially higher than at steady-state conditions, and thus decreases as a function of time to a steady-state rate. Possible explanations could be either (1) the rapid consumption of fine particles still adhering to the grains and/or (2) the rapid disappearance of the most reactive, high-energy lattice defects of the grains (e.g. the corner ledges of grains) (see e.g. Hellmann (1995) for a thorough discussion). In any case, this phenomenon of high initial rates is especially significant at far-from-equilibrium conditions (Fig. 1a, experiment DPS-B, $\Delta G_r = -105.8$ kJ mol^{-1}), and extends considerably the time needed to collect accurate, steady-state data. As an example, one can compare the expected time needed to reach steady-state chemical conditions based only upon a 'hydrodynamic steady-state' criterion of 2 or 3τ (where τ is the residence time, i.e. V/v). In the case of experiment DPS-B, this yields a duration of ~1.4–2.2 days, whereas the outlet concentration of solutes actually attains a plateau after $t > 17$ days. The initially fast dissolution rate is also presumably responsible for the existence of 'false' steady-state conditions, as already pointed out in e.g. Chen and Brantley (1998) for diopside and Hellmann and Tisserand (2006) for albite feldspar. An example of such 'false' steady-states is highlighted in Fig. 1a, where a steady-state concentration could be envisaged between days 11 and 14 of the experiment, while the outlet concentration actually achieves constancy (within the analytical uncertainties) only after 17 days. The difference between the two averaged values ('pseudo' steady-state vs. 'true' steady-state) is not dramatic, but remains measurable, however (~8%). In other kinetic studies in the literature, this difference could be more important.

In the transition ΔG_r regime (e.g. Fig. 1b, experiment DPS-F, $\Delta G_r = -68.2$ kJ mol^{-1}), the difference between the inlet and outlet concentrations is characterised by a monotonic increase with time (in contrast to experiments farther from equilibrium, where concentrations first attain a maximum before decreasing with time). The experimental data lie above the modelled curves, indicating that the initial apparent dissolution rate of diopside is faster than the dissolution rate at steady-state conditions. However, the theoretical time needed to reach a plateau (~50–60 days) is similar to the observed one (up to ~70 days, defined by concentrations remaining approximately constant).

Experiments run even closer to equilibrium (e.g. Fig. 1c, experiment DPS-J, $\Delta G_r = -55.7$ kJ mol^{-1}) required up to 100 days for the stabilisation of the outlet concentrations, and thus, for the determination of steady-state dissolution rates. Once again, the initial release of elements to the reactor

is faster than that predicted if the rate was constant with time. However, one can note that the difference between the initial slopes of the measured $\Delta[i](t)$ values (dotted line in Fig. 1a–c, represented only for Si) and the initial slopes of the calculated curves (solid blue line on Fig. 1a–c for Si) decreases as a function of the value of steady-state ΔG_r at which the experiment was conducted. This could indicate that initial non-steady-state dissolution rates decrease with increasing ΔG_r, which is the same behaviour as with the steady-state rates.

In summary, as noted by Hellmann and Tisserand (2006), the achievement of chemical steady-state rates is almost always longer than the 'hydrodynamic steady-state' criterion, and increases with increasing ΔG_r. This proves an essential point: the attainment of steady-state rates can never be assumed, and therefore always requires experimental confirmation.

3.2. Steady-state dissolution stoichiometry

3.2.1. General considerations

The steady-state behaviour of diopside dissolution as a function of ΔG_r can be characterised in terms of ratios of the aqueous cations released by diopside at the end of each experiment (i.e. [Ca]/[Mg]; [Ca]/[Si]; [Mg]/[Si]). In Fig. 2, the experimental ratios have been normalised by the corresponding ratios defined by the cation stoichiometry in diopside (henceforth quoted Ca:Mg; Ca:Si; Mg:Si). As a consequence, in this figure, stoichiometric release of any of the given pairs of cations corresponds to a value of 1.00 ± 0.05 (the confidence interval is based upon the analytical uncertainties in the measurements of the chemical composition of the diopside by electron microprobe, i.e. $\pm 5\%$). Considering in addition that each datum is affected by the analytical uncertainties in the measurements of aqueous concentration ($\pm 6\%$, corresponding to uncertainties of the ratios of $\pm 12\%$), the majority (72%) of the normalised ratios are situated within this confidence interval. Excluding Ca:Si and Mg:Si values determined in experiments DPS-K and DPS-L (conducted at $\Delta G_r = -50.3$ and -47.0 kJ mol^{-1}, respectively), as well as that of Ca:Mg determined in experiment DPS-L (justifications for this will be discussed in Section 3.2.2) increases to 82% the proportion of normalised ratios situated within the confidence interval of congruent dissolution, with mean values of 0.90, 0.95 and 1.10 for Ca:Mg, Ca:Si and Mg:Si, respectively. These results indicate that steady-state diopside dissolution is essentially congruent. A more precise interpretation of the observed ratios in each experiment based solely on the aqueous chemistry of the collected output fluids is rather risky. This will require detailed investigations at the nanoscale of the surface state of the altered grains (see e.g. high resolution TEM studies: Hellmann et al., 2003, 2004; Daval et al., 2009b); and will thus be explored in the upcoming study.

3.2.2. Was dissolution affected by secondary precipitation processes?

During the course of the experiment performed at conditions closest to equilibrium (DPS-L, $\Delta G_r = -47.0$ kJ mol^{-1}), it is clear that silica-bearing secondary phases precipitated because the inlet concentration of $SiO_2(aq)$ is
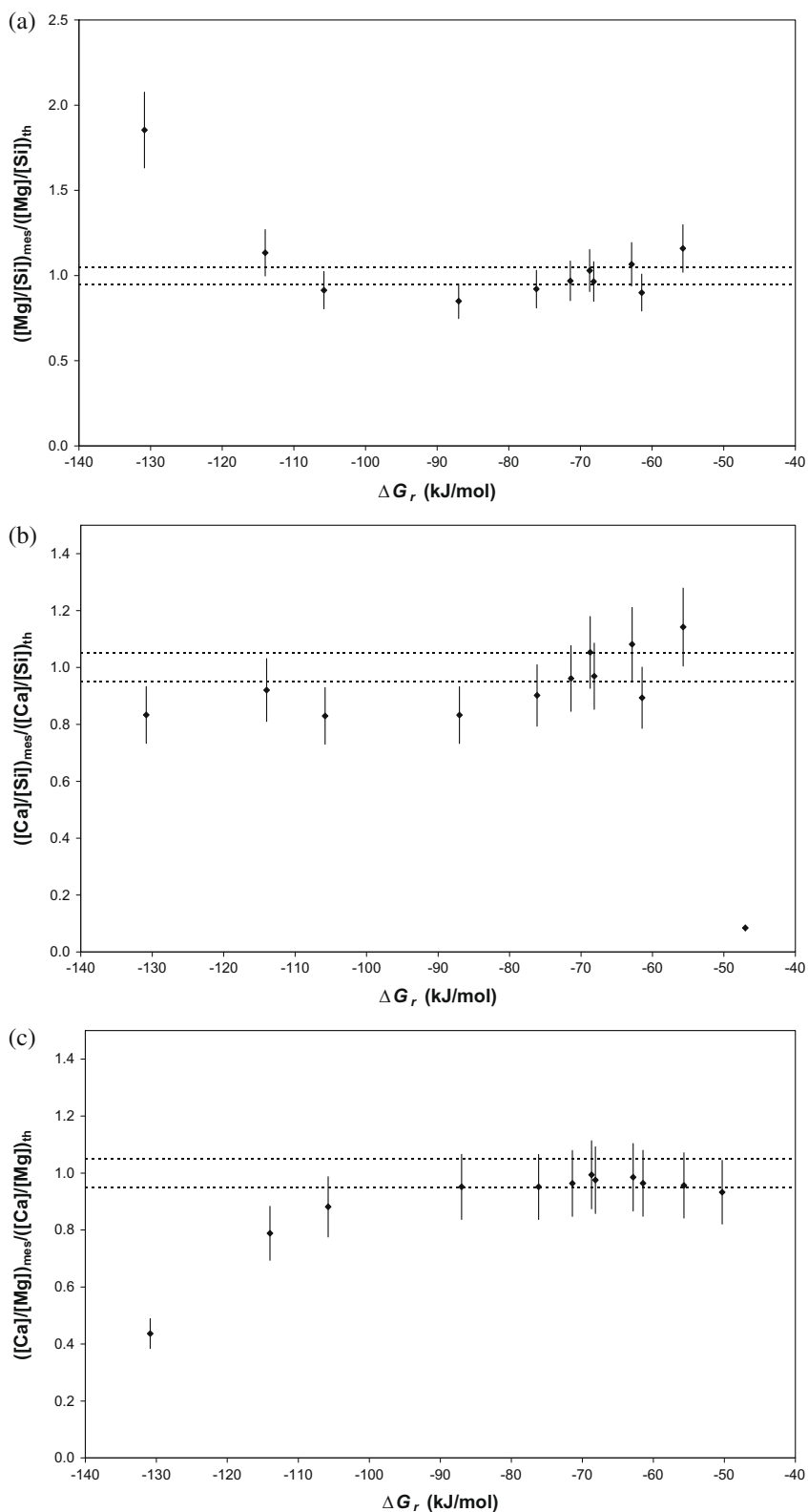
Fig. 2. Measured ratios of the aqueous cations released by diopside, normalised to the corresponding ratios defined by the cation stoichiometry in diopside, respectively (a) Mg:Si, (b) Ca:Si and (c) Ca:Mg. Each datum represents the last sample of an experimental run, or in certain cases, the last sample before a rate change occurred. The region between the dashed lines represents congruent dissolution. Note that most of the data fall within this region. On the other hand, the data collected closest to equilibrium (i.e. DPS-K and DPS-L, $\Delta G_r \geqslant -50$ kJ mol^{-1}) were affected by precipitation of silica in the outlet tubing (see text for details) and cannot be represented in this figure. The gap between experimental Mg:Si and Ca:Mg ratios and theoretical ones at $\Delta G_r = -131$ kJ mol^{-1} is attributed to Mg contamination (see Table 2).

greater than the corresponding outlet concentration (see Table 2 for details). Moreover, it is likely that some of the secondary phases that formed during the course of this experiment also contained Ca, since $\Delta[Ca] < 0$ as well. However, there was no evidence of any secondary μm-sized crystals occurring on the reacted diopside grain surfaces, based on SEM (further details can be found in Daval, 2009). The aim of the present section is thus to enlighten whether the precipitation of the secondary phases was thermodynamically possible, both at *in situ* conditions (i.e. in the autoclave) or at room temperature (i.e. in the Ti tubing), as a consequence of the difference of solubility of secondary phases as a function of temperature.

To unravel the origin of this observed non-stoichiometry, CHESS was used to determine ΔG_r values with respect to the formation of secondary phases, based on the measured output solution compositions for the three experiments conducted closest to equilibrium (DPS-J, DPS-K and DPS-L). The thermodynamic EQ 3/6 database that we used was updated with the equilibrium constants of calcium–silicate–hydrate (C–S–H) determined by Corvisier et al. (2009). The saturation states of the fluids were calculated both at $T = 90\ °C$ and $T = 20\ °C$ (i.e. room temperature). The calculated Gibbs free energies of precipitation of secondary phases (Table 3, negative values thereby indicating that precipitation is feasible) were either based on the fluid analyses (detailed in Table 2) or on theoretical fluid compositions assuming stoichiometric diopside dissolution. For the experiments conducted closest to equilibrium (i.e., DPS-J, DPS-K and DPS-L), the fluid was only found to be close to saturation or supersaturated with respect to SiO_2 polymorphs and C–S–H phases (those with the lowest Ca to Si ratio) at 20 °C, which are thus the only phases reported in Table 3. Most importantly, it can be noticed that at 90 °C, the solutions were not supersaturated with respect to amorphous silica and C–S–H, regardless of the way in which the fluid compositions were defined (i.e. measured compositions, or theoretical stoichiometric compositions based on Mg release). This is obviously all the more true for experiments DPS-A to DPS-I, because they were run at conditions even further from equilibrium. As a consequence, it is likely that

at 90 °C, the experiments were not affected by any secondary precipitation process, as previous experiments showed that among SiO_2 polymorphs, only amorphous silica precipitation is relatively rapid (see e.g. Rimstidt and Cole, 1983; Giammar et al., 2005; and discussion in Daval et al., 2009a) and that the other silica polymorphs which could thermodynamically form in these experiments do not precipitate for kinetic reasons. In addition, the solution was near saturation or supersaturated with respect to amorphous silica in all of the three experiments (DPS-J, DPS-K and DPS-L) at 20 °C, and close to saturation with respect to C–S–H phases with Ca:Si $\leqslant 0.05$ for experiments DPS-K and DPS-L at 20 °C. The precipitation of such phases within the cold outlet Ti tubing of the apparatus is thus the presumable explanation which can account for the apparent non-stoichiometry of diopside dissolution. Moreover, after DPS-L experiment, it was verified that flushing this tubing with an acidic solution resulted in the release of significant amounts of $SiO_2(aq)$, whereas that of Ca was weaker ($\sim$8% of $SiO_2(aq)$), and that of Mg was insignificant. Such trends were not observed by flushing the inlet tubing, confirming that precipitation in the cold part of the apparatus likely occurred in the outlet tubing only.

To conclude, these observations suggest that the dissolution process which occurred at 90 °C was not affected *in situ* by any secondary precipitates. As discussed by e.g. Burch et al. (1993) or Hellmann and Tisserand (2006), this is an important point, as significant secondary precipitation can greatly complicate the interpretation of the observed decrease in the dissolution rates of parent minerals.

3.3. Steady-state dissolution rates as a function of ΔG_r

3.3.1. Overall r–ΔG_r relation

The steady-state rates of dissolution as a function of ΔG_r are shown in Fig. 3a–c. For each investigated ΔG_r, Fig. 3a and Table 2 represent the individual rates based upon the Ca, Mg and Si concentrations measured at the end of each run (or for non-zero input solutions, based on $\Delta[i]$); these

Table 3
Gibbs free energy of precipitation (in kJ mol^{-1}) for secondary phases for the 3 experiments conducted the closest to equilibrium.

Experiment	T (°C)		Quartz	Tridymite	Chalcedony	Cristobalite (α)	Coesite	Cristobalite (β)	SiO$_2$ (am)	CSH005	CSH010
DPS-J	20	(a)	−7.37	−6.38	−5.82	−4.22	−2.75	−1.65	0.06	2.78	4.38
	90	(a)	−2.62	−1.48	−1.07	0.38	2.07	2.58	3.85	5.84	6.18
DPS-K	20	(a)	−9.36	−8.37	−7.81	−6.20	−4.74	−3.64	−1.92	0.31	2.62
		(b)	−9.52	−8.53	−7.97	−6.37	−4.90	−3.80	−2.09	−0.09	2.48
	90	(a)	−5.08	−3.94	−3.54	−2.08	−0.39	0.12	1.39	3.48	3.88
		(b)	−5.28	−4.14	−3.74	−2.28	−0.59	−0.08	1.19	3.27	3.70
DPS-L	20	(a)	−9.18	−8.19	−7.63	−6.03	−4.56	−3.46	−1.75	0.76	1.68
		(b)	−9.61	−8.63	−8.07	−6.46	−5.00	−3.90	−2.18	−0.54	2.99
	90	(a)	−4.87	−3.72	−3.32	−1.86	−0.18	0.34	1.61	3.88	4.10
		(b)	−5.40	−4.26	−3.85	−2.40	−0.71	−0.20	1.07	3.41	3.82

The calculations were based either (a) on the exact results of fluid analyses (see Table 2) or (b) on a fluid composition corresponding to a stoichiometric release of elements, when the reaction was found to be strongly incongruent (i.e. experiments DPS-K and DPS-L). The solid phases labelled CSH005 and CSH010 correspond to C–S–H that have Ca over Si ratios equal to 0.05 and 0.10, respectively (see text and Corvisier et al. (2009) for details).
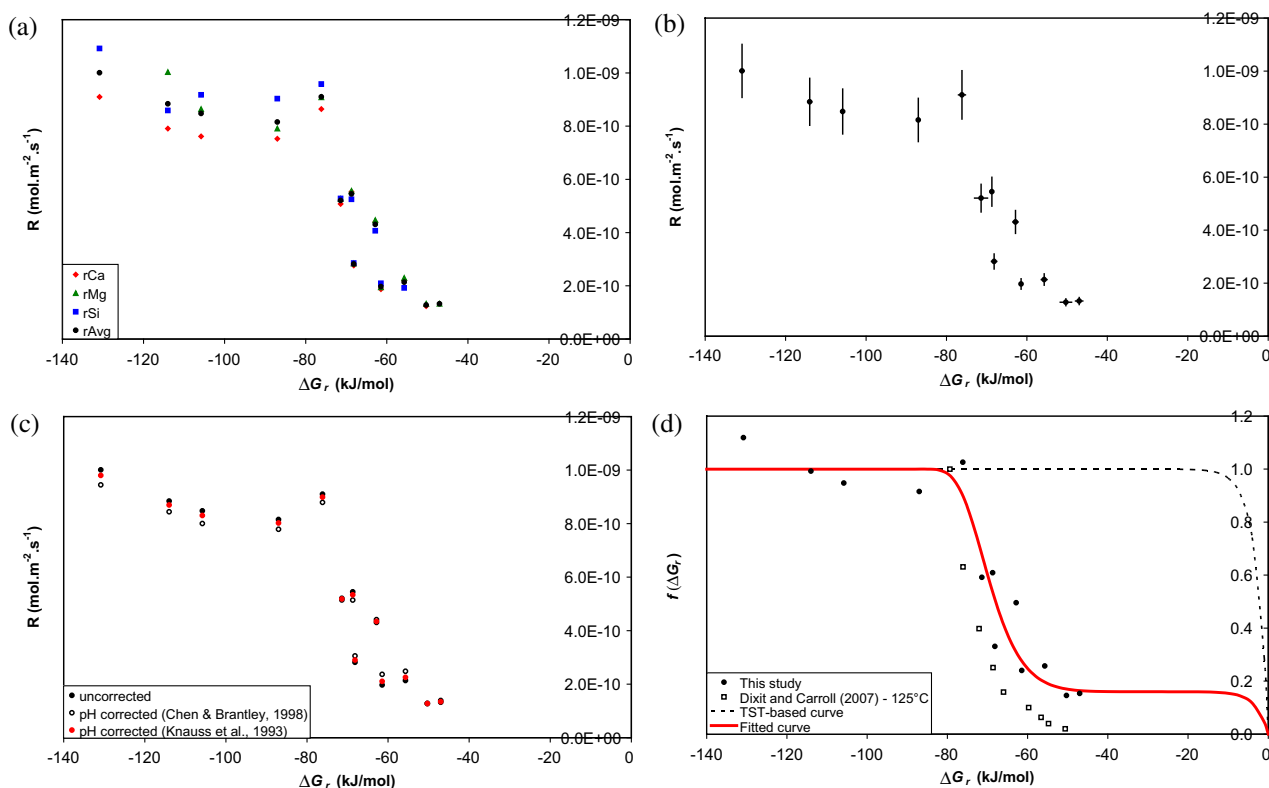
Fig. 3. Entire dissolution rate-Gibbs free energy of dissolution (ΔG_r) data set collected in the present study. (a) Measured rates of diopside dissolution r_{Ca}, r_{Mg} r_{Si}, and unweighted mean r_{Avg} (see legend) as a function of ΔG_r. (b) Average rates with standard deviations based only on the analytical uncertainties in the ICP-AES measurements, thus showing the relative errors between data. The uncertainties in ΔG_r were based on the uncertainties in the ICP-AES measurements and in the *in situ* pH determinations. The five rates measured farthest from equilibrium are consistent with the existence of a rate plateau. (c) Original (i.e. uncorrected) average dissolution rates, intrinsically affected by slight pH variations from one experiment to another, and corrected average dissolution rates corrected for these pH variations using pH-dependences reported in the literature (see text and legend). The overall behaviour of the r–ΔG_r data is clearly not affected by these small adjustments. (d) The pH-corrected rates (using the pH-dependency of Knauss et al. (1993) - see text for details) and the fitted rate curve show that the r–ΔG_r relation is highly non-linear and sigmoidal). The abrupt drop of r with ΔG_r between $\sim$−76 and −60 kJ mol^{-1} is in good accord with the normalised data of Dixit and Carroll (2007), whereas both data sets and the fitted curve are at odds with the TST-based curve.

rate data have not been modified by any data processing (with just one exception: because of significant analytical uncertainty in [Mg] for experiment DPS-A1, r_{Mg} is not shown and the mean dissolution rate corresponding to $\Delta G_r = -130.9$ kJ mol^{-1} is only based on r_{Ca} and r_{Si}). Fig. 3a also shows the average dissolution rates (r_{Avg}), where each rate is based on the unweighted mean of the three rates (r_{Ca}, r_{Mg} and r_{Si}), except for experiments in which the effluent concentration was affected by presumed silica (and C–S–H) precipitation in the outlet tubing (see Section 3.2.2 and Table 2 for details). The overall dataset covers an extensive range of Gibbs free energy of >80 kJ mol^{-1}, which represents, as far as we know, the largest continuous range of ΔG_r studied with respect to diopside dissolution kinetics.

Because of the weak buffering capacity of the acetate solution that was used in the present study (in order to maintain low acetate concentrations; as explained in Section 2.3, diopside dissolution behaviour is supposedly unaffected when the concentration of acetate ligands is low), the pH of the reactor solutions was slightly affected by the con-

sumption of H$^+$ during diopside dissolution, and ranged between 4.95 (experiment DPS-A1) and 5.16 (experiment DPS-G). As a consequence, the mean rates (Fig. 3a and b) were corrected for these pH variations using previously published studies that determined the pH-dependence of diopside dissolution rates. All the dissolution rates of our study were recalculated to a normalised rate based on the *ad hoc* choice of pH 5.00. The mean rates were normalised using either the acid pH-dependence determined by Knauss et al., 1993 (i.e. $n = 0.19$) or that from Chen and Brantley, 1998. Note, however, that Chen and Brantley (1998) normalised all the measured rates to the final surface area of diopside after dissolution. For internal consistency with the present study, where all the rates were normalised to the initial surface area, the pH-dependence was recalculated from their data determined at 90 °C and normalised to the initial surface area given in their study. This treatment yields a value of $n = 0.51$ (the regression coefficient being $r^2 = 0.993$). Our rate data were thus subsequently corrected using either $n = 0.19$ or $n = 0.51$, with the results shown in Fig. 3c. Strikingly, the overall behaviour of the r–ΔG_r data-

set is not affected by these very small adjustments, the corrected rates remaining largely within the error bars of the dissolution rates shown in Fig. 3b. Consequently, the slight pH variations from one experiment to another have an insignificant effect on the determined rates and are not responsible for the variation of the rates.

Taken together, the data in Fig. 3a–c define a highly non-linear relation between r and ΔG_r. At far-from-equilibrium conditions ($\Delta G_r < -76$ kJ mol^{-1}), a rate plateau is observed. The mean plateau rate defined by the five average rates for $-130.9 < \Delta G_r < -76$ kJ mol^{-1} is (1) $8.92 \pm 1.09 \times 10^{-10}$; (2) $8.76 \pm 1.75 \times 10^{-10}$; (3) $8.50 \pm 1.88 \times 10^{-10}$ mol m^2 s^{-1} based respectively on (1) the uncorrected rate values, (2) the pH-corrected values using data from Knauss et al. (1993), (3) the pH-corrected values using data from Chen and Brantley (1998). These mean plateau rates can be compared with far-from-equilibrium rates derived from the literature. Extrapolations from the studies of Knauss et al. (1993) and Chen and Brantley (1998) (data normalised to initial surface area) yield $r^{T=90\,^\circ C}_{pH=5.00} = 6.96 \times 10^{-10}$ mol m^2 s^{-1} and $r^{T=90\,^\circ C}_{pH=5.00} = 2.94 \times 10^{-11}$ mol m^2 s^{-1}, respectively. Whereas the former value from Knauss et al. (1993) is in excellent agreement with the 3 mean plateau rates determined in our study, more than one order of magnitude difference exists with the extrapolated value from Chen and Brantley (1998). Possible explanations for such discrepancies have been discussed by Chen and Brantley (1998), although they pointed out that it was not possible to unambiguously determine the reason for these major inconsistencies.

Referring back to the overall behaviour of the r–ΔG_r dataset, three distinct regions can be evidenced. The region defined by $\Delta G_r \leqslant -76.2$ kJ mol^{-1} represents far-from-equilibrium dissolution (see above) and a rate plateau. In the plateau region, the dissolution rates are constant and independent of ΔG_r. Such rate plateaus have also been evidenced for a wide variety of minerals like quartz (e.g. Berger et al., 1994), feldspars (Schott and Oelkers, 1995 (anorthite); Taylor et al., 2000 (labradorite); Burch et al., 1993; Hellmann and Tisserand, 2006; Hellmann et al., in press (albite)), clays (e.g. Nagy et al., 1991 (kaolinite); Cama et al., 2000 (smectite)), gibbsite (Nagy and Lasaga, 1992), or magnesite (Pokrovsky and Schott, 1999). To the best of our knowledge, our study is the first to unambiguously demonstrate the occurrence of a rate plateau at far-from-equilibrium conditions with respect to dissolution of diopside. It is interesting to note that in the diopside dissolution study by Dixit and Carroll (2007), a rate plateau was not reported. However, since only one of their experiments was conducted at $\Delta G_r < -76$ kJ mol^{-1} (see their Table 2), there is no apparent contradiction between their results and the ones reported here.

The second region, often called the 'transition region' (e.g. Hellmann and Tisserand, 2006), is characterised by an abrupt drop of the dissolution rates over a narrow range of ΔG_r ($-76.2 < \Delta G_r \leqslant -61.5$ kJ mol^{-1}), thus indicating a strong inverse dependence of the rates on free energy. This observation is in reasonable agreement with the results obtained by Dixit and Carroll (2007) at 125 °C, where a similar strong inverse dependence of the rates on ΔG_r up to -59.72 kJ mol^{-1} was determined. To better illustrate this

agreement, their data at 125 °C were normalised by supposing that their rate obtained at -79.36 kJ mol^{-1} (experiment 125-1) was representative of far-from-equilibrium conditions (i.e. according to our results, $f(\Delta G_r = -79.36) = 1$, the normalised rate) and compared with the normalised dissolution rates of the present study (our rate data were all normalised to an unweighted mean of the 5 rate values over the free energy range -130.9 kJ mol$^{-1} \leqslant \Delta G_r \leqslant -76.2$ kJ mol^{-1}). The good correspondence in the narrow free energy range where the dissolution rates decrease dramatically can be seen in Fig. 3d. On the other hand, the experiments conducted by Dixit and Carroll (2007) at higher temperatures cannot be compared with the ones obtained in the present study because their investigations did not measure rates at free energies of less than -37 kJ mol^{-1} (i.e. their experiment 150-A1), such that it was not possible to normalise the corresponding data to a far-from-equilibrium, ΔG_r-independent rate value.

Dissolution closest to equilibrium, defined by $\Delta G_r > -61.5$ kJ mol^{-1}, represents the 'near equilibrium' region where the rates decrease with increasing free energy as chemical equilibrium is approached. In this region, the inverse dependence of the rates on the free energy is much weaker than in the transition region. Unfortunately, due to the experimental difficulties already described above (i.e. precipitation of secondary phases in the outlet tubing, as well as the limited pH buffering capacity of acetate), it was not possible to realise experiments at $\Delta G_r > -47.0$ kJ mol^{-1}. Thus, the behaviour of the r–ΔG relation between -47.0 kJ mol^{-1} and theoretical equilibrium remains unknown. Note that the normalised data of Dixit and Carroll (2007) (Fig. 3d) suggest that the dissolution rates may continue to decrease gradually over this range of free energy ($\Delta G_r > -61.5$ kJ mol^{-1}).

On the whole and consistently with Dixit and Carroll's study, one of the most important results of our study is the occurrence of a steep drop of the dissolution rate at very negative ΔG_r values. Even if, in the worst (unlikely) case scenario, the three lowest affinity experiments were considered to be compromised by precipitation (DPS-J, DPS-K and DPS-L, see Section 3.2.2), this finding is unaffected by this concern at least on the free energy range < -60 kJ mol^{-1}.

3.3.2. Reconsidering what 'far-from equilibrium conditions' means

Our data complement results from a growing number of studies dealing with the effect of solution saturation state on mineral dissolution. One important point in particular is clearly revealed here: our results suggest that the commonly found term in dissolution studies, "far-from-equilibrium conditions", is perhaps overused and should indeed be used with caution. Authors have often used the aforementioned term to 'define' dissolution conditions sufficiently far-from-equilibrium, such that ΔG_r has no influence on the rate, and that the $f(\Delta G_r)$ term can be safely omitted from a given rate law (i.e. $f(\Delta G_r) = 1$). This assumption is largely based on the idea that basic TST-free energy relations predict that rate plateaus begin at free energy values of a few kJ mol^{-1} only (for example, at 90 °C, $f(\Delta G_r) > 0.95$ as long as

$\Delta G_r < -10$ kJ mol^{-1}, as can be calculated using Eq. (2)). However, as it is clearly seen in the present study, the r–ΔG_r behaviour of our experimental data is highly incompatible with the r–ΔG_r relation based on such basic TST models (see Eq. (2); dotted line in Fig. 3d). Thus, reliance on TST-free energy relations may prove to be erroneous for several reasons, and in particular, with respect to predicting where the onset of a rate plateau occurs. From the present study, we show that free energies greater than -76 kJ mol^{-1} do not represent what would classically be defined as far-from-equilibrium conditions for diopside dissolution. Hence, without a priori knowledge of the r–ΔG_r relation for diopside (or any other particular mineral), a rate measured at a ΔG_r value of -75 kJ mol^{-1} may be erroneously considered to represent a rate at 'far-from-equilibrium' conditions and a rate plateau.

Indeed, as noted by Dixit and Carroll (2007), dissolution rate plateaus can be reached over a broad range of free energy values, from a few kJ mol^{-1} (e.g. -5 kJ mol^{-1} for gibbsite, Nagy and Lasaga, 1992) to several tens of kJ mol^{-1} for other minerals (e.g. -50 kJ mol^{-1} for labradorite, Taylor et al., 2000; -76 kJ mol^{-1} for diopside, present study). This could have major implications with respect to the interpretation of several previously published studies, and in particular, those dedicated to the pH-dependence of silicate mineral dissolution over an extended range of pH. As we detailed earlier (Section 2.6), ΔG_r depends strongly on a_{H^+}. Because of this, at basic pH conditions, it can be 'analytically challenging' to execute dissolution studies at very low ΔG_r values (e.g. for diopside, $\Delta G_r < -76$ kJ mol^{-1}) simply due to the difficulty of measuring extremely low concentrations of cations such as Ca, Mg and Si. Thus, rate values obtained at basic pH may, in fact, correspond to ΔG_r values that are not rate plateau values. If this is the case, then comparison with rates obtained at acidic pH (where it is far easier to obtain rates at very low ΔG_r values corresponding to a rate plateau) would lead to erroneous extended r–pH relations. Fig. 4 schematically buttresses these arguments by way of an example based on diopside dissolution. This figure shows that at pH greater than ~8.20, the typical analytical limits of ICP-AES measurements of released cations (i.e. [Ca], [Mg], [Si]) correspond to ΔG_r values greater than -76 kJ mol^{-1}. Interestingly, it has been found that diopside dissolution exhibits a monotonic decrease of the logarithm of the dissolution rate with increasing pH from 2 to 12 (e.g. Knauss et al., 1993), in contrast with many silicates which display classical 'U-shaped' r–pH relations.

Besides, silicates which exhibit 'U-shaped' r–pH relations are, in their vast majority, Al-bearing silicates, such as albite (e.g. Chou and Wollast, 1984), microcline (Schweda, 1989), muscovite (e.g. Knauss and Wolery, 1989), kaolinite (e.g. Carroll and Walther, 1990), biotite (e.g. Malmström and Banwart, 1997), chlorite (Lowson et al., 2005). It is interesting to notice that for Al-bearing silicates, a fixed cationic fluid composition (corresponding to the chemistry of the Al-bearing silicate) yields increasingly negative ΔG_r values as pH increases (see Fig. 4, using albite as an example). Thus, measuring ΔG_r-independent dissolution rates of Al-bearing silicates at basic pH should be technically feasible. In contrast, for numerous Al-free/(Ca, Mg, Fe)-rich minerals, r was observed not to increase as a function of pH at basic conditions (e.g. wollastonite (Xie and Walther, 1994); enstatite (Oelkers and Schott, 2001); diopside (Knauss et al., 1993); olivine (Pokrovsky and Schott, 2000); talc (Saldi et al., 2007)). As for such minerals, ΔG_r values increase as pH increases, it can be questioned whether all the reported dissolution rates at basic pH actually fell on the 'far-from-equilibrium' rate plateau (i.e. rates independent of ΔG_r).
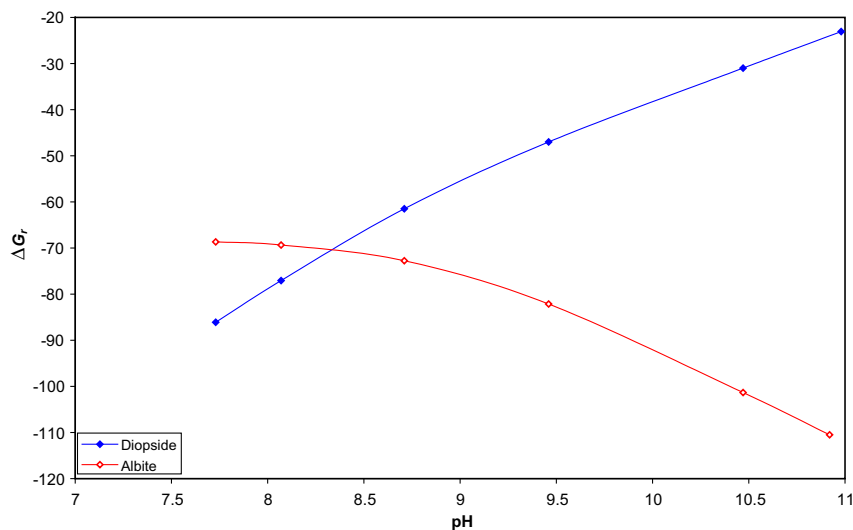

Fig. 4. Gibbs free energy of dissolution computed as a function of pH for a constant fluid composition corresponding to conditions close to estimated analytical limits of ICP-AES measurements. The blue symbols represent diopside and red albite. The calculations were based on a theoretical fluid composition including a NaOH/H$_3$BO$_3$ buffer (0.043 mol l^{-1} NaOH, variable amounts of H$_3$BO$_3$) and fixed concentrations of cations (for diopside [Ca] = [Mg] = [Si]/2 = 0.25 µM; for albite [Al] = [Si]/3 = 0.25 µM). (For interpretation of colour mentioned in this figure, the reader is referred to the web version of this article.)

3.3.3. Numerical fit of the experimental data

As emphasised by Lüttge (2006) and Casey (2008), rate data from macroscopic measurements are generally not precise enough to uniquely define a given reaction mechanism. Macroscopic data, such as those presented here, can be fitted by empirical rate laws that are useful for predictive purposes (see Section 3.4), but cannot easily provide insights into the reaction mechanisms at a molecular level. Indeed, in this study, the ΔG_r parameter is rather used as a control parameter of the dissolution experiment without an *a priori* idea about its mechanism of action. Several possibilities can be envisaged but, whatever the case, the precise deciphering of the reaction mechanisms will require investigations at a submicrometric scale, which is the main subject of an ongoing companion study. Our main concern in the present study is to adequately fit the observed r–ΔG_r relation and to examine its main geochemical consequences.

The curve fitting strategy we adopted was largely influenced by the similarities that exist between the behaviour of our r–ΔG_r data and those from previous studies (in particular, Burch et al., 1993; Taylor et al., 2000; Hellmann and Tisserand, 2006). As described above, the overall r–ΔG_r data exhibit non-linear, sigmoidal behaviour for which several authors (e.g. Burch et al., 1993) have proposed fitting relations. To explain the sigmoidal trends of the $f(\Delta G_r)$ function, the authors of these studies have proposed that the driving process of dissolution should be the spontaneous nucleation of etch pits at crystal defects (screw dislocations) when $\Delta G_r < \Delta G_r^{crit}$, where ΔG_r^{crit} is the critical free energy required for opening an etch pit at a given crystal defect (e.g. Lüttge, 2006). This critical free energy corresponds to the onset of a transition free energy region. Above ΔG_r^{crit}, it is predicted that deep etch pits should not open up spontaneously, and this, in turn, would explain the slow dissolution rates observed in the range $\Delta G_r^{crit} < \Delta G_r < 0$. A similar approach was applied to r–ΔG_r studies by Lasaga and co-workers and applied in many other studies that show non-linear, sigmoidal r–ΔG_r behaviour (e.g. Nagy and Lasaga, 1992 (gibbsite); Burch et al., 1993 (albite); Cama et al., 2000 (smectite); Taylor et al., 2000 (labradorite), Hellmann and Tisserand, 2006; Hellmann et al., in press (albite)).

One way to take into account mathematically the dependence of a dissolution process controlled by a critical free energy (postulated in the present study to be comprised between -76.2 and -61.5 kJ mol^{-1}, since this range in ΔG_r corresponds to the transition region characterised by a sharp change in the rates of dissolution) is to write $f(\Delta G_r)$ as the sum of two separate parallel processes (e.g. Burch et al., 1993, see also Taylor et al., 2000 and Hellmann and Tisserand, 2006):

$$f(\Delta G_r) = k \times \left[1 - \exp\left(-\alpha \times \left(\frac{|\Delta G_r|}{RT} \right)^{\beta} \right) \right] + (1 - k)$$
$$\times \left[1 - \exp\left(-\frac{|\Delta G_r|}{RT} \right) \right]^{\gamma} \qquad (11)$$

where k, α, β and γ are fitted coefficients, the latter three having no physical meaning. The k term of the expression above represents the normalised rate constant at far-from-

equilibrium conditions $\Delta G_r < \Delta G_r^{crit}$, whereas the $(1 - k)$ term equals the normalised rate that predominates at close-to-equilibrium (i.e. at $\Delta G_r^{crit} < \Delta G_r < 0$). The coefficients k, α, β were determined by regression to be equal to 0.84; 8.5×10^{-18}, and 12.41, respectively (root mean square: 0.09); because of the lack of data near equilibrium, the γ parameter was simply set to unity. Note that this assumption is in reasonable agreement with the results published by Taylor et al. (2000) for labradorite ($\gamma = 1$) and Hellmann and Tisserand (2006) for albite ($\gamma = 1.17$). The fitted curve obtained with these parameters, shown in Fig. 3d (red line), is sigmoidal and highly non-linear. The consequences of the significant deviation of this curve from the TST-based one are detailed below using an example based on carbonation reactions (Section 3.4).

A final point that we discuss concerns the sigmoidal shape of the $f(\Delta G_r)$ function. In the present study, the experimental data show quite good continuity, extending from conditions at far-from-equilibrium, traversing the transition region, and continuing at closer to equilibrium conditions. However, the interpretation of data in the transition region has been debated in recent publications (e.g. Beig and Lüttge, 2006; Lüttge, 2006). According to these studies, any rate data falling in this steep transition region represent non-steady-state phenomena, and can be attributed to experimental protocol or 'sample history' (i.e. initiation of experiments at far-from-equilibrium conditions). Etch pits formed during the initial stages of dissolution at conditions far-from-equilibrium would continue to promote the process in the transition region, such that the apparent dissolution rates measured would be greater than their 'true' values. In other words, they propose that the dissolution rate jumps to the plateau rate in a discontinuous manner (i.e. the r–ΔG_r function is not sigmoidal, but rather a step-like function). We note that in the present study, all the rate data falling in the transition region were indeed obtained from experiments initiated at conditions which can be considered as to be 'far-from-equilibrium' (either at $\Delta G_r \rightarrow -\infty$ (i.e. experiments DPS-E, DPS-F and DPS-G), or at $\Delta G_r = -77$ kJ mol^{-1} (i.e. experiments DPS-H and DPS-I), see Table 2 for details). On the other hand, Dixit and Carroll (2007) showed that experimental protocol did not significantly impact dissolution rates measured. In summary, this controversy points out that more experimental work needs to be done in order to verify or disprove this idea.

3.4. Implications for geochemical modeling – application to carbonation reactions

In this paragraph, we investigate the consequences of the r–ΔG_r relation that we measured for diopside dissolution on the geochemical modeling of the carbonation reaction of this mineral. For this purpose, we developed a calculation module implemented in a classical geochemical code. Let us consider the following simplified formalism:

$$A \rightarrow B \rightarrow C \qquad (12a)$$

In a carbonation reaction, 'A' represents the reactants, i.e. (ultra)basic silicate mineral and H_2CO_3, 'B', the aqueous

species released during dissolution (see e.g. Eq. (4)), and 'C', the product phases, which include solid carbonates and amorphous silica. In the Earth sciences, such types of reactions have received attention because of a 'cooperative' autocatalytic effect (see e.g. review in Putnis, 2002). In Eq. (12a), the rapid consumption of B is responsible for ensuring that reaction A → B cannot approach equilibrium. In fact, Daval et al. (2009a) demonstrated that although wollastonite is one of the most reactive Ca-bearing minerals (see their Fig. 7), during carbonation reactions, its dissolution rate remains far slower than the process of calcite and amorphous silica formation (phases C in Eq. (12a)), such that Eq. (12a) can be re-written as follows:

$$A \rightarrow B \leftrightharpoons C \tag{12b}$$

As a consequence, the solution composition and ΔG_r with respect to the reaction A → B (which is rate-limiting for the overall process) will remain roughly constant during the carbonation reaction. This observation justifies the need for an accurate $f(\Delta G_r)$ function, as this parameter is one of the crucial points for determining whether carbonation is a viable process for sequestering CO_2 efficiently, as has been commonly suggested (e.g. Lackner, 2003; Oelkers et al., 2008). Other factors as well can also play an important role in carbonation, such as possible passivation of the dissolution reaction by solid phases that precipitate around the primary silicate mineral grains, thereby diminishing the rate of the global process (for carbonation reactions, see e.g. Shih et al., 1999; Park and Fan, 2004; Béarat et al., 2006; Stockmann et al., 2008; Daval et al., 2009a,b). This phenomenon will not be further considered here in order to focus primarily on rate-free energy effects.

The quantitative determination of the potential overestimation of carbonation rates using generally available geochemical codes (where the vast majority of these codes base the $f(\Delta G_r)$ function on standard TST) was assessed by bypassing the kinetic module of CHESS (van der Lee and de Windt, 2002). Instead, an alternative kinetic module was developed and coupled with the thermodynamic module of CHESS. In this kinetic module, the temporal evolution of the primary silicate mineral undergoing dissolution was solved using the Newton–Raphson method. As one can show, determining the amount of silicate remaining at time $t + \Delta t$ (mol^{i+1}) as a function of the initial amount of silicate present at time t (mol^i) is based on:

$$mol^{i+1} = mol^i - \frac{f(mol^i)}{f'(mol^i)} \tag{13}$$

where $f(mol^i)$ is defined by:

$$f(mol^i) = mol^i - mol^{i-1} - \Delta t \times r^i \tag{14}$$

such that:

$$f'(mol^i) = 1 - \Delta t \times \frac{\partial r^i}{\partial mol^i} \tag{15}$$

In the equations above, r^i represents the silicate dissolution rate at time t expressed in mol s^{-1} (note that $r^i < 0$ as mol decreases as a function of time). The expression for r^i follows from a simplification of Eq. (1):

$$r^i = -k_0 \times \exp(-E_a/RT) \times (a_{H^+}^i)^n \times f(\Delta G_r^i) \times A_{min}^i \tag{16}$$

The definitions of the different parameters used in this equation are the same as already described earlier for Eq. (1), the only difference being their variability with time, as symbolised by the superscript 'i'. Finally, for internal consistency with the initial kinetic module of the CHESS code, A_{min}^i was linked to mol^i by the relation:

$$A_{min}^i = SSA_0 \times mol^i \tag{17}$$

where SSA_0 represents the initial specific surface area (e.g. determined by Kr-BET) expressed in m^2 mol^{-1}. After each kinetic loop, the amount of mineral loss to the solution is translated in terms of the aqueous components released to the solution. These data are used together with the temperature and the CO_2 fugacity (f_{CO_2}) as input for the thermodynamic module of the CHESS code, which calculates the speciation of the aqueous phase, as well as the potential precipitation of secondary phases, and yields in turn the updated values of $a_{H^+}^{i+1}$ and ΔG_r^{i+1} that are used as inputs for the next kinetic step.

This coupled code was used to simulate the extents of diopside carbonation as a function of time, using either (1) Eq. (2) (i.e. the TST-based law) or (2) Eq. (11) that utilised the fitted parameters determined in the present study. The other major rate-controlling parameters of diopside dissolution (pH-dependence, dissolution rate constant, and activation energy) were taken from the study of Knauss et al. (1993). Based on previous studies dedicated to mineral carbonation of basalts and pyroxenes (which included diopside), the long-term carbonation of diopside at conditions relevant to CO_2 sequestration (e.g. $T = 90\,°C$ and $f_{CO_2} = 13$ MPa) should occur as follows (e.g. Dufaud, 2006; McGrail et al., 2006, and references therein; Stockmann et al., 2008):

$$CaMgSi_2O_6 + 2CO_2 \rightarrow CaMg(CO_3)_2 + 2SiO_2(am) \tag{18}$$
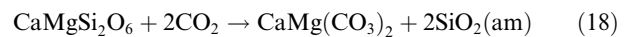
The precipitation kinetics of the solid phases that were allowed to precipitate (i.e. $CaMg(CO_3)_2$ and $SiO_2(am)$) were defined in terms of infinitely rapid rates (i.e. equilibrium with solution phase). If this assumption is justified for phases such as calcite or SiO_2 (am) (see Daval et al., 2009a for details), this is more questionable with respect to dolomite precipitation ($CaMg(CO_3)_2$), for which data are scarce (e.g. Arvidson and Mackenzie, 2000). However, note that this choice ensures that the fluid is not artificially constrained to attain the ΔG_r^{crit} value previously mentioned, and thus dissolution is not forced to occur at the slowest ΔG_r regime. As a consequence, the differences between the simulations using respectively TST and actual r–ΔG_r data can be considered as a lower bound for the overestimation of carbonation rates determined by the use of the TST-based free energy relation. The simulations were performed with an arbitrary mass of diopside of 300 mg (i.e. 1.4 mmol) and $SSA_0 = 0.028$ m^2/g, and were initiated in 0.5 mL of pure water (leading to a high rock/water ratio, as is the case in confined subsurface systems). The normalised extents of diopside carbonation were calculated using the following relation:

$$\xi = n_{dol}/n_{dps}^0 \tag{19}$$

where n_{dol} is the total amount of dolomite formed after a given time and n_{dps}^0 the initial amount of diopside.

The results of these simulations are shown in Fig. 5a. First of all, and not surprisingly one can note the perfect agreement between the modelled curves generated using either the CHESS code or our kinetic module implemented with the TST-based free energy relation. This observation warrants the correctness of our module. Secondly, the discrepancies between these two curves and the one obtained implementing the $f(\Delta G_r)$ function determined in the present study are striking. The time needed to reach completion of the carbonation reaction using CHESS and the TST module is less by a six-fold factor compared to the parallel rate law module. As explained above and illustrated in Fig. 5b, this is due to the fact the reaction quickly attains $\Delta G_r = \Delta G_r^{crit}$, despite the fact that $B \leftrightarrows C$. Note that the specific assumption of infinite rate of dolomite formation (i.e. when comparing to diopside dissolution) will require further research but that the rapid precipitation of calcite instead of dolomite, leaving Mg ions in solution, would not drastically change the conclusions drawn here (see Daval (2009) for further details and calculations). In any case, in order to completely overcome this dolomite question, the modeling was extended to the case of labradorite, another

Ca-bearing silicate for which non TST r–ΔG_r data have been reported (Taylor et al., 2000). The dissolution rate law of labradorite, including the pH-dependence, the dissolution rate constant, and the activation energy, was taken from the study of Sjöberg (1989); the $f(\Delta G_r)$ function was that from Taylor et al. (2000). The secondary phases formed during labradorite carbonation were estimated from experiments dedicated to the weathering of feldspars under high pCO$_2$. A compilation of studies from Carroll and Knauss, 2005 (labradorite), Regnault et al., 2005 (anorthite), Hellmann et al., in press (albite), suggest that the reaction of labradorite with CO$_2$ should lead to the formation of gibbsite (Al(OH)$_3$), kaolinite (Al$_2$Si$_2$O$_5$(OH)$_4$), calcite, and amorphous silica. For the same reasons as those described above, the precipitation kinetics of the solid phases was defined in terms of infinitely rapid rates. The equilibrium constant (K_{eq}) for labradorite was calculated supposing an ideal solid solution between albite and anorthite feldspars. Equilibrium constants for albite and anorthite were taken from the EQ3/6 database. The simulations were performed with an arbitrary mass of labradorite of 375 mg (i.e. 1.4 mmol) and SSA$_0$ = 0.028 m^2/g. The results (Fig. 5c) also evidence that the basic TST law yields significantly shorter times for reaching completion
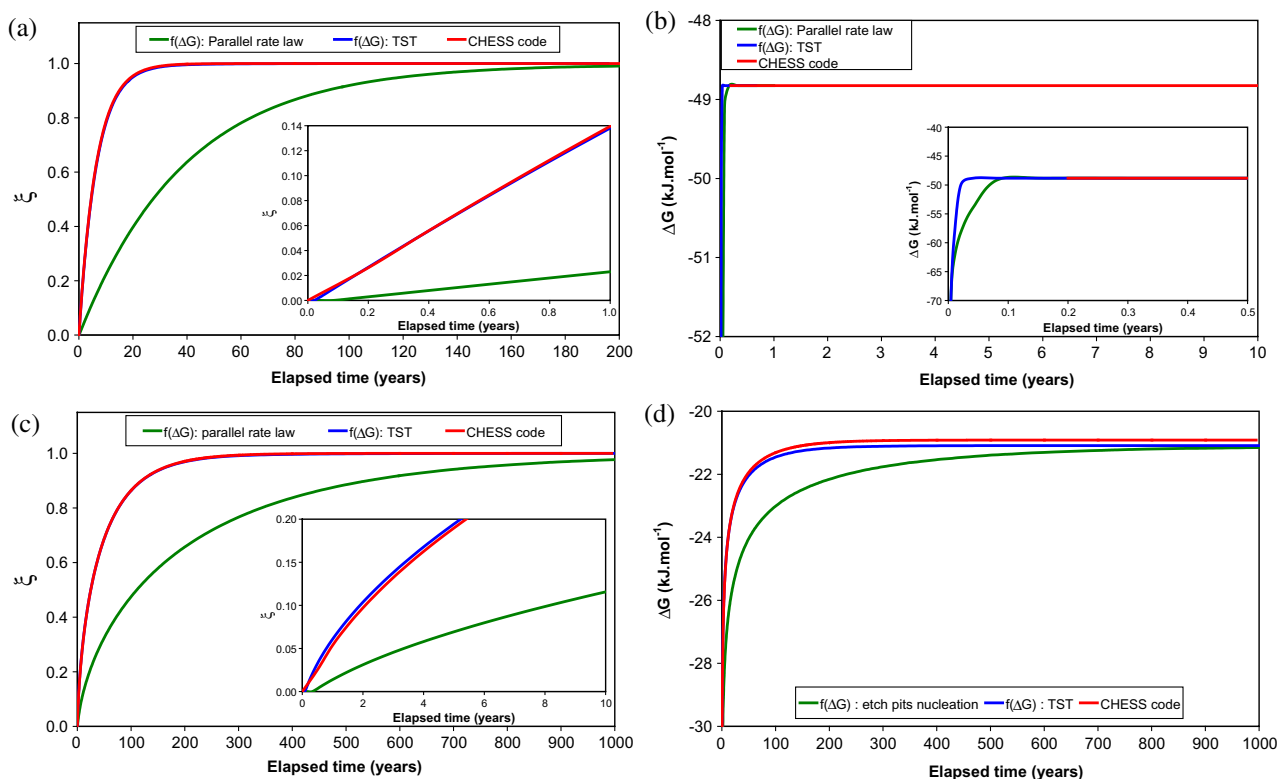

Fig. 5. Kinetic modeling of diopside carbonation reaction. For all four graphs, the green and blue curves were obtained using a kinetic module coupled to the thermodynamic one of the CHESS code; the $f(\Delta G_r)$ relations are either based on TST (blue) or the experimental results (green). The red curve was obtained using just the CHESS code. Graphs (a) and (c) represent extents of diopside (a) and labradorite (c) carbonation as a function of time. Note that the use of $f(\Delta G_r)$ relations based on TST predict significantly higher extents of reaction over the indicated time periods. The insets show the early stages of the carbonation process. Graphs (b) and (d) represent the calculated evolution of the Gibbs free energy of diopside (b) and labradorite (d) dissolution as a function of time. In each case, ΔG_r quickly attains a plateau value – see text for details). (For interpretation of colour mentioned in this figure, the reader is referred to the web version of this article.)

of carbonation, largely due to the fact that the main part of the reaction takes place at $\Delta G_r > \Delta G_r^{crit}$ (Fig. 5d).

The impact of these results on numerical simulations of CO_2 sequestration by solid carbonate formation is thus potentially important. With respect to carbonation reactions, if the existence of a ΔG_r^{crit} value is confirmed for other dissolution reactions involving M^{2+}-bearing silicates, the use of general geochemistry codes that use TST-based free energy relations will remain satisfactory only for carbonation reactions that occur at fluid saturations implying $\Delta G_r < \Delta G_r^{crit}$. In that case, dissolution will take place on the r–ΔG_r plateau, whatever the $f(\Delta G_r)$ function, so that the dissolution rate will be independent of ΔG_r. Such questions underline the need for additional experimental investigations on mineral dissolution rate/free energy relationships. In the absence of these fundamental and specific data, any modeling efforts dealing with the long-term evolution of water–CO_2–rocks interactions (e.g. Xu et al., 2004; Knauss et al., 2005) should be considered prone to large errors.

4. CONCLUSIONS

One of the most important conclusions of the present study is the very abrupt decrease of the dissolution rate of diopside from a rate plateau far-from-equilibrium to significantly lower rates, occuring at relatively large degrees of undersaturation, over a ΔG_r range between -76.2 and $-61.5 \text{ kJ mol}^{-1}$. This overall behaviour between r and ΔG_r, which precludes an interpretation based on a classical TST-free energy relation, has at least two important implications. First, a re-examination of the data dealing with the pH-dependence of diopside from circum-neutral to basic pH is needed, as such data cannot be easily obtained experimentally at ΔG_r values which could be considered to represent 'far-from-equilibrium' (rate plateau) conditions. This finding could be generalised to other M^{2+}-bearing/Al-free minerals (such as enstatite or forsterite), if similar r–ΔG_r behaviour was confirmed. Second, the deviation of the $f(\Delta G_r)$ function determined in the present study from the TST-based one, which is used in the vast majority of geochemical codes, suggests that numerical simulations of water–rock interactions should be evaluated with great caution; this was illustrated in the present study with respect to carbonation reactions. The societal problem of anthropogenic atmospheric CO_2, and the concomitant proposed solutions for mitigating it, which include geological sequestration of CO_2, is among those fields of study which heavily rely on modeling, and for which the experimental determination of r–ΔG_r relations will be necessary. In fact, on a more general scale, the extrapolation of experimental dissolution rates to the field scale will similarly require such studies.

The rate data in the present study cover an extensive range of free energies (80 kJ mol^{-1}), although there is a lack of data for $\Delta G_r > -47 \text{ kJ mol}^{-1}$. Experimentation closer to equilibrium will almost certainly be challenging due to the complexities associated with unravelling the dissolution rate signal from the effects of highly likely precipitation of secondary phases. Finally, the overall behaviour between

r and ΔG_r resembles closely that of several previously published studies, where it was suggested that the sigmoidal behaviour is attributable to parallel rate processes controlled by a critical free energy and its relation to the spontaneous opening up of deep etch pits. However, mechanistical interpretations of macroscopic data from reactor-based studies are fraught with difficulties. The most promising approach is rather based on detailed measurements of altered grains at the μm to nm-scale. This question will thus be addressed in an upcoming study.

REFERENCES

Aagaard P. and Helgeson H. C. (1982) Thermodynamic and kinetic constraints on reaction-rates among minerals and aqueous-solutions. 1. Theoretical considerations. *Am. J. Sci.* **282**, 237–285.

Arvidson R. S. and Mackenzie F. T. (2000) Temperature dependence of mineral precipitation rates along the $CaCO_3$–$MgCO_3$ join. *Aquat. Geochem.* **6**, 249–256.

Bachu S. (2002) Sequestration of CO_2 in geological media in response to climate change: road map for site selection using the transform of the geological space into the CO_2 phase space. *Energy Convers. Manage.* **43**, 87–102.

Béarat H., McKelvy M. J., Chizmeshya A. V. G., Gormley D., Nunez R., Carpenter R. W., Squires K. and Wolf G. H. (2006) Carbon sequestration via aqueous olivine mineral carbonation: role of passivating layer formation. *Environ. Sci. Technol.* **40**, 4802–4808.

Beig M. S. and Luttge A. (2006) Albite dissolution kinetics as a function of distance from equilibrium: implications for natural feldspar weathering. *Geochim. Cosmochim. Acta* **70**, 1402–1420.

Berger G., Cadore E., Schott J. and Dove P. M. (1994) Dissolution rate of quartz in lead and sodium electrolyte solutions between 25 and 300 °C: effect of the nature of surface complexes and reaction affinity. *Geochim. Cosmochim. Acta* **58**, 541–551.

Brantley S. L. (1992) Kinetics of dissolution and precipitation – experimental and field results. In *Water–Rock Interaction* (eds. Y. K. Kharaka and K. A. Maest). Balkema, Rotterdam, pp. 3–6.

Brantley S. L. and Chen Y. (1995) Chemical weathering rates of pyroxenes and amphiboles. In *Chemical Weathering Rates of Silicate Minerals* (eds. A. F. White and S. L. Brantley). Mineralogical Society of America, Pennsylvania State University.

Burch T. E., Nagy K. L. and Lasaga A. C. (1993) Free energydependence of albite dissolution kinetics at 80 °C and pH 8.8. *Chem. Geol.* **105**, 137–162.

Cama J., Ganor J., Ayora C. and Lasaga A. C. (2000) Smectite dissolution kinetics at 80 °C and pH 8.8. *Geochim. Cosmochim. Acta* **64**, 2701–2717.

Carroll S. A. and Knauss K. G. (2005) Dependence of labradorite dissolution kinetics on CO_2(aq), Al(aq), and temperature. *Chem. Geol.* **217**, 213–225.

Carroll S. A. and Walther J. V. (1990) Kaolinite dissolution at 25 °C, 60 °C, and 80 °C. *Am. J. Sci.* **290**, 797–810.

Casey W. H. (2008) Glass and mineral corrosion: dynamics and durability. *Nat. Mater.* **7**, 930–932.

Casey W. H., Westrich H. R., Massis T., Banfield J. F. and Arnold G. W. (1989) The surface of labradorite feldspar after acid hydrolysis. *Chem. Geol.* **78**, 205–218.

Chen Y. and Brantley S. L. (1998) Diopside and anthophyllite dissolution at 25 and 90 °C and acid pH. *Chem. Geol.* **147**, 233–248.

Chou L. and Wollast R. (1984) Study of the weathering of albite at room-temperature and pressure with a fluidized-bed reactor. *Geochim. Cosmochim. Acta* **48**, 2205–2217.

Corvisier J., Brunet F., Morales-Florez V. and Goffé B. (2009) A new thermodynamic model for C–S–H solubility valid in the range of P–T conditions encountered around CO_2-injection wells. *Geochim. Cosmochim. Acta* **73**, A244.

Daval, D. (2009) Processus de carbonatation de basaltes et de roches ultrabasiques en conditions de subsurface. Ph. D. thesis, Univ. Paris 7, p. 418 pp.

Daval D., Martinez I., Corvisier J., Findling N., Goffé B. and Guyot F. (2009a) Carbonation of Ca-bearing silicates, the case of wollastonite: experimental investigations and kinetic modeling. *Chem. Geol.* **265**, 63–78.

Daval D., Martinez I., Guigner J.-M., Hellmann R., Corvisier J., Findling N., Dominici C., Goffé B. and Guyot F. (2009b) Mechanism of wollastonite carbonation deduced from micro-to nanometer length scale observations. *Am. Mineral.* **94**, 1707–1726.

Davis M. C., Wesolowski D. J., Anovitz L. M., Allard L. F., Brantley S. L. and Mueller K. T. (2008) Near-equilibrium investigations of quartz and forsterite dissolution. *Geochim. Cosmochim. Acta* **72**, A202.

Devidal J.-L., Schott J. and Dandurand J.-L. (1997) An experimental study of kaolinite dissolution and precipitation kinetics as a function of chemical affinity and solution composition at 150 °C, 40 bars, and pH 2, 6.8, and 7.8. *Geochim. Cosmochim. Acta* **61**, 5165–5186.

Dixit S. and Carroll S. A. (2007) Effect of solution saturation state and temperature on diopside dissolution. *Geochem. Trans.* **8**.

Drever J. I. and Clow D. W. (1995) Weathering rates in catchments. In *Chemical Weathering Rates of Silicate Minerals* (eds. A. F. White and S. L. Brantley). Mineralogical Soc. America, Washington, pp. 463–484.

Dufaud, F. (2006) Etude expérimentale des réactions de carbonatation minérale du CO_2 dans les roches basiques et ultrabasiques. Institut de Physique du Globe de Paris.

Eggleston C. M., Hochella, Jr., M. F. and Parks G. A. (1989) Sample preparation and aging effects on the dissolution rate and surface composition of diopside. *Geochim. Cosmochim. Acta* **53**, 797–805.

Eyring H. (1935a) The activated complex and the absolute rate of chemical reactions. *Chem. Rev.* **17**, 65–82.

Eyring H. (1935b) The activated complex in chemical reactions. *J. Phys. Chem.* **3**, 107–120.

Gautier J. M., Oelkers E. H. and Schott J. (1994) Experimental-study of K-feldspar dissolution rates as a function of chemical affinity at 150 °C and pH 9. *Geochim. Cosmochim. Acta* **58**, 4549–4560.

Giammar D. E., Bruant R. G. and Peters C. A. (2005) Forsterite dissolution and magnesite precipitation at conditions relevant for deep saline aquifer storage and sequestration of carbon dioxide. *Chem. Geol.* **217**, 257–276.

Goddéris Y., Francois L. M., Probst A., Schott J., Moncoulon D., Labat D. and Viville D. (2006) Modelling weathering processes at the catchment scale: the WITCH numerical model. *Geochim. Cosmochim. Acta* **70**, 1128–1147.

Golubev S. V. and Pokrovsky O. S. (2006) Experimental study of the effect of organic ligands on diopside dissolution kinetics. *Chem. Geol.* **235**, 377–389.

Hänchen M., Prigiobbe V., Storti G., Seward T. M. and Mazzotti M. (2006) Dissolution kinetics of fosteritic olivine at 90–150 °C. *Geochim. Cosmochim. Acta* **70**, 4403–4416.

Hellmann R. (1995) The albite-water system Part II: the time-evolution of the stoichiometry of dissolution as a function of pH at 100, 200, and 300 °C. *Geochim. Cosmochim. Acta* **59**, 1669–1697.

Hellmann R. and Tisserand D. (2006) Dissolution kinetics as a function of the Gibbs free energy of reaction: an experimental study based on albite feldspar. *Geochim. Cosmochim. Acta* **70**, 364–383.

Hellmann R., Dran J. C. and Della Mea G. (1997) The albite–water system. 3: characterization of leached and hydrogen-enriched layers formed at 300 °C using MeV ion beam techniques. *Geochim. Cosmochim. Acta* **61**, 1575–1594.

Hellmann R., Penisson J.-M., Hervig R. L., Thomassin J.-H. and Abrioux M.-F. (2003) An EFTEM/HRTEM high-resolution study of the near surface of labradorite feldspar altered at acid pH: evidence for interfacial dissolution–reprecipitation. *Phys. Chem. Mineral.* **30**, 192–197.

Hellmann R., Penisson J.-M., Hervig R. L., Thomassin J.-H. and Abrioux M. F. (2004) Chemical alteration of feldspar: a comparative study using SIMS and HRTEM/EFTEM. In *Water–Rock Interaction* (eds. R. B. Wanty and IIR. R. Seal). A.A. Balkema, pp. 753–756.

Hellmann R., Daval D., Tisserand D. and Renard F. (2007) Albite feldspar dissolution kinetics as a function of the Gibbs free energy at high pCO_2. In *Water–Rock Interaction* (eds. T. D. Bullen and Y. Wang). Taylor and Francis, pp. 591–595.

Hellmann, R., Daval, D. and Tisserand, D. (in press) The dependence of albite feldspar dissolution kinetics on fluid saturation state at acid and basic pH: progress towards a universal relation. *C. R. Geosci*, doi:10.1016/j.crte.2009.06.004.

Knauss K. G. and Wolery T. J. (1989) Muscovite dissolution kinetics as a function of ph and time at 70 °C. *Geochim. Cosmochim. Acta* **53**, 1493–1501.

Knauss K. G., Nguyen S. N. and Weed H. C. (1993) Diopside dissolution kinetics as a function of pH, CO_2, temperature, and time. *Geochim. Cosmochim. Acta* **57**, 285–294.

Knauss K. G., Johnson J. W. and Steefel C. I. (2005) Evaluation of the impact of CO_2, co-contaminant gas, aqueous fluid and reservoir rock interactions on the geologic sequestration of CO_2. *Chem. Geol.* **217**, 339–350.

Lackner K. S. (2003) A guide to CO_2 sequestration. *Science* **300**, 1677–1678.

Lasaga A. C. (1981) Transition state theory. In *Kinetics of Geochemical Process* (eds. A. C. Lasaga and R. J. Kirkpatrick). Mineralogical Society of America.

Lasaga A. C. (1995) Fundamental approaches in describing mineral dissolution and precipitation rates. In *Chemical Weathering Rates of Silicate Minerals* (eds. A. F. White and S. L. Brantley). Mineralogical Society of America.

Lasaga A. C. and Lüttge A. (2001) Variation of crystal dissolution rate based on a dissolution stepwave model. *Science* **291**, 2400–2404.

Lowson R. T., Comarmond M. C. J., Rajaratnam G. and Brown P. L. (2005) The kinetics of the dissolution of chlorite as a function of pH and at 25 °C. *Geochim. Cosmochim. Acta* **69**, 1687–1699.

Lüttge A. (2006) Crystal dissolution kinetics and Gibbs free energy. *J. Electron Spectrosc. Relat. Phenom.* **150**, 248–259.

Malmström M. and Banwart S. (1997) Biotite dissolution at 25 °C: the pH dependence of dissolution rate and stoichiometry. *Geochim. Cosmochim. Acta* **61**, 2779–2799.

McGrail P. B., Schaef T. H., Ho A. M., Chien Y.-J. and Dooley J. J. (2006) Potential for carbon dioxide sequestration in flood basalts. *J. Geophys. Res.* **111**, B12201.

Murakami T., Kogure T., Kadohara H. and Ohnuki T. (1998) Formation of secondary minerals and its effect on anorthite dissolution. *Am. Mineral.* **83**, 1209–1219.

Nagy K. L. and Lasaga A. C. (1992) Dissolution and precipitation kinetics of gibbsite at 80 °C and pH 3: the dependence on solution saturation state. *Geochim. Cosmochim. Acta* **56**, 3093–3111.

Nagy K. L., Blum A. E. and Lasaga A. C. (1991) Dissolution and precipitation kinetics of kaolinite at 80 °C and pH 3; the dependence on solution saturation state. *Am. J. Sci.* **291**, 649–686.

Nugent M. A., Brantley S. L., Pantano C. G. and Maurice P. A. (1998) The influence of natural mineral coatings on feldspar weathering. *Nature* **395**, 588–591.

Oelkers E. H. and Schott J. (2001) An experimental study of enstatite dissolution rates as a function of pH, temperature, and aqueous Mg and Si concentration, and the mechanism of pyroxene/pyroxenoid dissolution. *Geochim. Cosmochim. Acta* **65**, 1219–1231.

Oelkers E. H., Schott J. and Devidal J.-L. (1994) The effect of aluminum, pH, and chemical affinity on the rates of alumino-silicate dissolution reactions. *Geochim. Cosmochim. Acta* **58**, 2011–2024.

Oelkers E. H., Gislason S. R. and Matter J. (2008) Mineral carbonation of CO$_2$. *Elements* **4**, 333–337.

Pačes T. (1972) Chemical characteristics and equilibration in natural water–felsic rock–CO$_2$ system. *Geochim. Cosmochim. Acta* **36**, 217–240.

Park A.-H. A. and Fan L.-S. (2004) CO$_2$ mineral sequestration: physically activated dissolution of serpentine and pH swing process. *Chem. Eng. Sci.* **59**, 5241–5247.

Pokrovsky O. S. and Schott J. (1999) Processes at the magnesium-bearing carbonates/solution interface. II: kinetics and mechanism of magnesite dissolution. *Geochim. Cosmochim. Acta* **63**, 881–897.

Pokrovsky O. S. and Schott J. (2000) Kinetics and mechanism of forsterite dissolution at 25 °C and pH from 1 to 12. *Geochim. Cosmochim. Acta* **64**, 3313–3325.

Putnis A. (2002) Mineral replacement reactions: from macroscopic observations to microscopic mechanisms. *Mineral. Mag.* **66**, 689–708.

Regnault O., Lagneau V., Catalette H. and Schneider H. (2005) Étude expérimentale de la réactivité du CO$_2$ supercritique vis-à-vis de phases minérales pures. Implications pour la séquestration géologique de CO$_2$. *C. R. Geosci.* **337**, 1331–1339.

Rimstidt J. D. and Cole D. R. (1983) Geothermal mineralization I: the mechanism of formation of the beowawe, Nevada, siliceous sinter deposit. *Am. J. Sci.* **283**, 861–875.

Saldi G. D., Kohler S. J., Marty N. and Oelkers E. H. (2007) Dissolution rates of talc as a function of solution composition, pH and temperature. *Geochim. Cosmochim. Acta* **71**, 3446–3457.

Schott J. and Oelkers E. H. (1995) Dissolution and crystallization rates of silicate minerals as a function of chemical affinity. *Pure Appl. Chem.* **67**, 903–910.

Schott J., Berner R. A. and Sjöberg L. (1981) Mechanism of pyroxene and amphibole weathering–I: experimental studies of iron-free minerals. *Geochim. Cosmochim. Acta* **45**, 2123–2135.

Schweda P. (1989) Kinetics of alkali feldspar dissolution at low temperature. In *Water–Rock Interaction* (ed. D. L. Miles). A.A. Balkema, pp. 609–612.

Shih S. M., Ho C. S., Song Y. S. and Lin J. P. (1999) Kinetics of the reaction of Ca(OH)$_2$ with CO$_2$ at low temperature. *Ind. Eng. Chem. Res.* **38**, 1316–1322.

Sjöberg L. (1989) Kinetics and non-stoichiometry of labradorite dissolution. In *Water–Rock Interaction WRI-6* (ed. D. L. Miles). A.A. Balkema, pp. 639–642.

Stefánsson A. and Arnórsson S. (2000) Feldspar saturation state in natural waters. *Geochim. Cosmochim. Acta* **64**, 2567–2584.

Stockmann G., Wolff-Boenisch D., Gislason S. R. and Oelkers E. H. (2008) Dissolution of diopside and basaltic glass: the effect of carbonate coating. *Mineral. Mag.* **72**, 135–139.

Swoboda-Colberg N. G. and Drever J. I. (1993) Mineral dissolution rates in plot-scale field and laboratory experiments. *Chem. Geol.* **150**, 51–69.

Taylor A. S., Blum J. D. and Lasaga A. C. (2000) The dependence of labradorite dissolution and Sr isotope release rates on solution saturation state. *Geochim. Cosmochim. Acta* **64**, 2389–2400.

van der Lee, J. and De Windt, L. (2002) *CHESS Tutorial and Cookbook. Updated for Version 3.0.*, Paris.

Velbel M. A. (1993) Formation of protective surface layers during silicate-mineral weathering under well-leached, oxidizing conditions. *Am. Mineral.* **78**, 405–414.

White A. F. and Brantley S. L. (2003) The effect of time on the weathering of silicate minerals: why do weathering rates differ in the laboratory and field? *Chem. Geol.* **202**, 479–506.

Xie Z. and Walther J. V. (1994) Dissolution stoichiometry and adsorption of alkali and alkaline earth elements to the acid-reacted wollastonite surface at 25 °C. *Geochim. Cosmochim. Acta* **58**, 2587–2598.

Xu T., Apps J. A. and Pruess K. (2004) Numerical simulation of CO$_2$ disposal by mineral trapping in deep aquifers. *Appl. Geochem.* **19**, 917–936.

Associate editor: Roy A. Wogelius